Check for updates

NANO · MICRO small
www.small-journal.com

The Formation and Transformation of Low-Dimensional Carbon Nanomaterials by Electron Irradiation

Florian Banhart

Dedicated to Pulickel M. Ajayan on the occasion of his 60th birthday

Low-dimensional materials based on graphene or graphite show a large variety of phenomena when they are subjected to irradiation with energetic electrons. Since the 1990s, electron microscopy studies, where a certain irradiation dose is unavoidable, have witnessed unexpected structural transformations of graphitic nanoparticles. It is recognized that electron irradiation is not only detrimental but also bears considerable potential in the formation of new graphitic structures. With the availability of aberration-corrected electron microscopes and the discovery of techniques to produce monolayers of graphene, detailed insight into the atomic processes occurring during electron irradiation became possible. Threshold energies for atom displacements are determined and models of different types of lattice vacancies are confirmed experimentally. However, experimental evidence for the configuration of interstitial atoms in graphite or adatoms on graphene remained indirect, and the understanding of defect dynamics still depends on theoretical concepts. This article reviews irradiation phenomena in graphene- or graphite-based nanomaterials from the scale of single atoms to tens of nanometers. Observations from the 1990s can now be explained on the basis of new results. The evolution of the understanding during three decades of research is presented, and the remaining problems are pointed out.

1. Introduction

The discovery of the fullerenes in 1985[1] gave the go-ahead for unprecedented activities in the research on carbon materials and new species of nanoparticles. It is not that carbon nanomaterials were completely unknown at that time; sub-micron graphitic particles have already been noticed long before in electron microscopy studies.[2] Not much importance was attached to these species that just seemed to be a miniaturization of their macroscopic counterparts. However, the comparatively simple synthesis techniques of fullerenes[3] and geometrical models explaining their structure[1,4] led to the discovery of new classes of carbon nanoparticles such as nanotubes[5,6] or graphene.[7] While fullerenes did not find as many applications as it had first been believed, nanotubes and graphene received much more long-lasting interest. This is due to their unusual and extreme physical properties that made them more attractive for fundamental studies and more useful for technical applications.

The enormous potential of carbon in the creation of various nano-architectures is due to the ability of the carbon atom to form bonds in three different hybridization states. Bonding geometries in a 1D linear atom chain (sp^1), a hexagonal atom network in two dimensions (sp^2), or a tetrahedral lattice in three dimensions (sp^3) can be realized. The 2D graphene lattice is by far the most interesting, not only because of its extreme properties but also due to the almost unlimited geometrical topologies that can be designed with a perfect or defective hexagonal network. It can easily be curved and rolled up by forming cylindrical nanotubes. Non-hexagonal atom rings are possible and produce curvature in three dimensions with the formation of closed or open structures of positive or negative curvature. These non-hexagonal defects turned out to be the key for designing architectures with new geometries and creating unusual materials.[8,9]

Many carbon species have been discovered in transmission electron microscopy (TEM) studies, and this has indeed remained the most productive imaging and diffraction technique to determine their structure. Subsequently, it has been noticed that the unavoidable electron irradiation in the microscope sometimes led to remarkable changes in the structure or morphology of carbon nanoparticles.[10,11] This was unexpected because irradiation with electrons causes damage in the specimen and is mostly considered as destructive and avoided wherever possible.

Radiation effects in the TEM have already been a well-known problem since the beginning of the electron microscopy era.[12–14] The energetic electrons of the beam ionize atoms, break chemical bonds, or displace atoms from their positions and create

F. Banhart
Institut de Physique et Chimie des Matériaux, UMR 7504
Université de Strasbourg, CNRS
Strasbourg 67034, France
E-mail: florian.banhart@ipcms.unistra.fr

The ORCID identification number(s) for the author(s) of this article can be found under https://doi.org/10.1002/smll.202310462

© 2024 The Authors. Small published by Wiley-VCH GmbH. This is an open access article under the terms of the Creative Commons Attribution-NonCommercial-NoDerivs License, which permits use and distribution in any medium, provided the original work is properly cited, the use is non-commercial and no modifications or adaptations are made.

DOI: 10.1002/smll.202310462

vacancies or interstitial atoms. So, it came as a surprise when carbon nanomaterials turned out to be an example (not the first but one of the most striking) where constructive radiation effects lead to new morphologies and phases of nanoparticles. Irradiation and imaging with the same electron beam (of course not the same electrons) allow monitoring of the formation of defects and structural changes of the particles in real-time. Of particular value were certain technical innovations of in situ TEM such as heating elements, piezo-driven tip contacts, or environmental reaction cells that are integrated into the specimen stages of the TEM. Upon changing the temperature of the material, passing an electrical current through it, applying mechanical stress, or exposing it to a reactive atmosphere, specific alterations appeared. For the first time, it became possible to monitor the growth of carbon nanotubes or graphene under realistic conditions and at high spatial resolution.[15]

The availability of aberration-corrected TEMs facilitated studies at higher spatial resolution and led to worldwide activities in the microscopy of graphene and nanotubes. Modern developments of TEM and more recently STEM (Scanning TEM) opened new routes toward unprecedented image resolution approaching the 50 pm scale. Of equal importance was the possibility of focusing sub-Ångstrom beam spots onto the specimens. This is not only useful for imaging and elemental analysis at the single-atom level[16] but also for deliberately displacing preselected atoms. For the first time, structuring at the atom scale was achieved with electron beams, and the application of this technique to 2D-structures such as graphene turned out to be highly productive.[17] This is due to the fact that a free-standing layer of monoatomic thickness can be exposed to the electron beam. No overlap effects appear (such as in the projection of 3D materials onto the image plane), and the defect configuration is immediately getting visible. Studying free-standing monolayers of solids with aberration-corrected TEMs is indeed the ideal technique to visualize point defects. Seeing vacancies in crystals has remained an almost hopeless challenge for decades, but right this has been achieved in 2D materials. And the many different vacancy configurations in graphene layers made these studies particularly fruitful.

The high selectivity of the electron beam together with the ability of the graphene lattice to reconstruct around vacancies[18,19] are the reasons why this became such a productive research field where the activities are still going on today. Now that individual point defects such as vacancies or foreign atoms can be identified in TEM images, several models of defect formation in graphitic materials dating back to the 1960s and 1970s, where the irradiation of nuclear graphite was of interest, had to be corrected or even given up. Our ability to not only identify individual atomic defects but also to monitor their migration in a certain temperature range, led us to a very detailed (though not complete) picture of defect formation and annealing in graphene and graphitic materials.

This article reviews discoveries around carbon nanomaterials by the techniques of electron microscopy and electron irradiation. **Figure 1** shows a graphical summary of radiation effects from displacements of single carbon atoms to larger structural transformations. It is instructive to follow the evolution of our understanding of radiation effects in graphitic carbon through the past decades and to show how technical improvements in electron microscopy have changed the picture. The motivation for this review was the possibility of explaining discoveries dating back to the 1990s with new data that allow us to complete the picture, albeit some open problems remain.

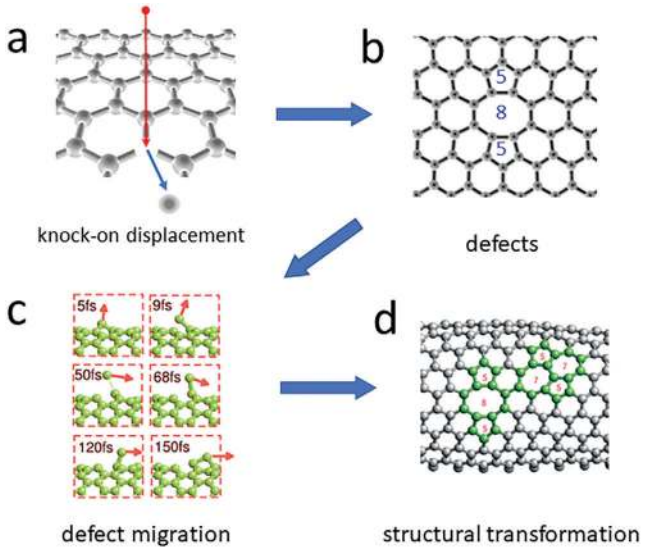

Figure 1. Schematic summary of irradiation effects in carbon nanomaterials. a): Carbon atoms are displaced from their lattice positions by momentum transfer in collisions with energetic electrons. b): Reconstruction of the graphene lattice around a double vacancy. c): Migration of ad-atoms on the surface of a carbon nanotube[20] (reproduced with permission, copyright 2005 American Physical Society). d): Shape transformation of a carbon nanotube after the formation of irradiation-induced vacancies.[18] c) and d): courtesy A. Krasheninnikov.

Since this is a concise review, a complete overview of the whole work on radiation effects in carbon materials cannot be given here. The focus is on graphitic nanomaterials such as graphene, carbon nanotubes, or other multi-shell graphitic particles where electron irradiation shows interesting phenomena. Diamond or other carbon phases will not be reviewed. Likewise, defects that are not important in irradiation (e.g., due to plastic deformation) will not be considered. The focus will be on experimental work and only those theoretical results closely related to experimental observations are cited.

2. Interaction between Energetic Electrons and Carbon Materials

Electron irradiation effects in the electron microscope are based on electron–electron scattering or on electron–nucleus scattering in the sample.[12,14] Inelastic electron–electron scattering events cause electronic excitation, plasmons (that dissipate into phonons), local ionization and the breaking of bonds. The scattering cross-section is a measure for the number of scattering events per second and increases with decreasing energy of the beam electron.[13] Therefore, radiation damage due to ionization (which is known as radiolysis) is more important at lower acceleration voltages of the microscope. However, the presence of conduction electrons in the material quenches ionization effects immediately so that radiolysis only occurs in insulators.

© 2024 The Authors. Small published by Wiley-VCH GmbH

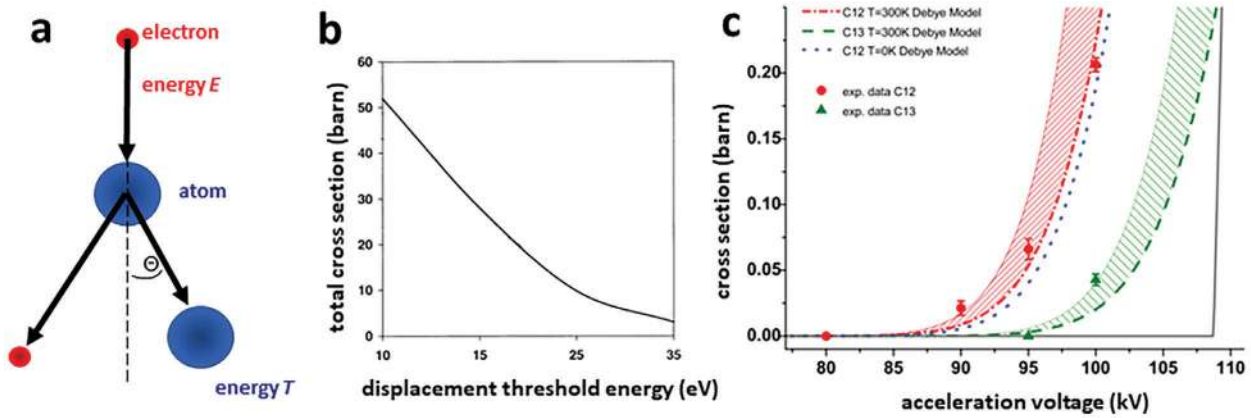

Figure 2. a): Geometry of the atom displacement. b): Displacement cross-section as a function of the threshold energy (calculated by using the McKinley-Feshbach formalism for an electron energy of 200 keV).[24] c): Displacement cross-section as a function of the acceleration voltage of the electron microscope.[23] Experimental (dots) and theoretical (lines) values are given for the two carbon isotopes ^{12}C and ^{13}C. c): Courtesy U. Kaiser, reproduced with permission, copyright 2012 American Physical Society.

Inelastic electron-nucleus scattering causes the displacement of atoms from their positions (**Figure 2a**) and can generally occur in all materials (side note: *elastic* electron-nucleus scattering does not result in an energy loss of the electron and is used for imaging or diffraction). The energy transfer T depends on the scattering angle Θ between the impinging electron and the direction into which the atom is scattered: $T(\Theta) = T_{max} \cos^2\Theta$ (Figure 2a, T is the energy transferred to the atom which reaches its maximum for a head-on collision at $\Theta = 0$). The scattering cross-section is based on the theory of Mott scattering and described by the McKinley-Feshbach formalism[21] which gives the displacement cross-section as a function of the maximum energy transfer. The displacement rate p is the product of the displacement cross-section σ and the beam current density j. To ensure a permanent atom displacement, i.e., the removal of the atom from its position without immediate relaxation of the interstitial-vacancy pair, a certain threshold energy is needed.[22] The displacement threshold energy depends on the mass of the atoms (it is higher for heavier elements), on the strength of bonding, and the crystal structure. The temperature of the material is also an important parameter in two different aspects. On the one hand, lattice vibrations facilitate atom displacements at higher temperatures[23] while, on the other hand, the mobility of interstitials and vacancies increases with temperature so that spontaneous annealing of interstitial-vacancy pairs may occur at higher temperatures. A higher electron energy is needed to displace atoms in a densely-packed crystal (e.g., diamond) than in an open structure (e.g., graphite). Furthermore, the displacement rate depends on the direction of the impinging electrons relative to the lattice orientation. The creation of a stable interstitial atom is easier if the atom is knocked toward an open space in the crystal than toward a neighboring atom.

Momentum conservation allows to establish a simple relation between the threshold energy of the beam electron E (typically tens or hundreds of keV) and the energy T_{max} that is transferred to the displaced atom (typically some eV or tens of eV):

$$T_{max} = \frac{2E\left(E + 2m_e c^2\right)}{Mc^2} \quad (1)$$

where m_e is the mass of the electron, M is the mass of the atom, and c is the speed of light (Figure 2a). The threshold T is orders of magnitude lower than E due to momentum conservation and the much lower electron mass compared to the mass of the displaced atom. It must be emphasized that the threshold energy of the displaced atom is not equal to the vacancy formation energy in the respective material (as sometimes assumed misleadingly). The anisotropy of the threshold within the lattice and spontaneous annealing effects have to be taken into account so that the threshold energy is higher than the vacancy formation energy. A detailed experimental determination of the displacement threshold is often indispensable.

One- and 2D carbon phases such as nanotubes, carbyne, or graphene have delocalized π-electrons that act as conduction electrons. Therefore, electron–electron scattering does not lead to considerable damage, and atom displacements are the principal source of structural transformations under the beam.[24] Single-layer graphene has the highest imaginable anisotropy of the lattice (unlimited open space normal to the direction of neighboring atoms), so atom displacements in graphene are easy if momentum transfer is normal to the layer and difficult if the displacement direction is parallel to the layer.

3. Atom Displacements

3.1. The Formation of Radiation Defects under Electron Irradiation

Much work has been devoted to the study of atom displacements in the different phases of carbon.[23–28] The studies date back to the 1960s when defects and radiation damage were studied in graphite as a material for nuclear reactors. The catastrophic release of the Wigner energy, when previously irradiated graphite is heated and sudden defect recombination occurs,[29] turned out to be a major safety issue in fission reactors with graphite moderators. However, at that time, the techniques of detecting defects were rather indirect (e.g., measurements of the electrical resistance or the stored energy), and the reported values of defect concentration and displacement rates or thresholds were not

© 2024 The Authors. Small published by Wiley-VCH GmbH

very reliable (an overview of the threshold energies measured by different techniques is given by Vucovic et al.).[28]

Nowadays, modern techniques of TEM allow the imaging of individual vacancies in graphene and single-wall carbon nanotubes. A precise measurement of the displacement threshold is possible by varying the acceleration voltage of the TEM and observing the formation of atomic defects in real-time. The knowledge of the displacement threshold is of importance for structure determination studies because these have to be carried out at an electron energy below the displacement threshold to avoid radiation damage. On the other hand, for studying radiation defects and the morphological restructuring of carbon nanoparticles, electron energies above the threshold are needed.

High-resolution TEM studies have been using a wide range of electron energies. To minimize the effect of spherical aberration and so to improve the achievable resolution of the microscopes, the acceleration voltage was raised from 100 kV in the 1960s to 400 kV in the 1980s and finally to >1000 kV in the 1990s. However, damage in the specimen due to ballistic atom displacements and displacement cascades increases with the electron energy, and this caused a reversal of the trend toward lower acceleration voltages. The availability of aberration correctors after the turn of the millennium allowed unprecedented image resolution in the sub-Ångstrom regime at voltages of 200 – 300 kV. With the first TEM studies of monolayer graphene, it was noticed that electron energies of 200 keV still cause displacements of carbon atoms, and calls for high-resolution microscopes with even lower voltages have been made. In the wake of the activities on graphene, aberration-corrected TEMs with acceleration voltages down to 20 kV were developed.[30] It is interesting to see how such a technical development was initiated by the discovery of new materials such as graphene or other low-dimensional systems.

The formation energy for monovacancies in graphite is 7.4 eV,[31] which is much higher than in most other materials such as in many metals. As a consequence, the concentration of vacancies in thermal equilibrium up to the melting or sublimation temperature of graphite is negligible. Irradiation of graphene, carbon nanotubes, or other graphitic nanomaterials in the TEM does not lead to a considerable temperature rise in the sample due to the low deposited energy.[12] From the migration of defects under the electron beam, an analogy with a high-temperature state has been assumed,[32] but it has later been shown that this is not an adequate model to describe radiation effects.[33] Whereas purely thermal effects occur in equilibrium, irradiation leads to a highly non-equilibrium state of the lattice. The amount of radiation damage in the sample can be quantified by the number of displacements per atom (dpa) during the irradiation period. The complexity of the processes after the primary atom displacement such as non-thermal recombination, cascades, or atom mixing, called for a refined model that was developed a few years ago.[34]

3.2. Displacement Threshold Energy

The displacement threshold energy is of high importance in TEM studies. Old studies in reactor graphite revealed too high values; e.g. a threshold electron energy of $E = 150$ keV (corresponding to an energy transfer of $T = 34$ eV to the displaced atom) along the c-axis at 600 °C was obtained by observing the appearance of defect clusters.[26] Meanwhile, detailed lattice imaging studies of graphene are available as well as theoretical studies of the threshold energies and displacement cross-sections for carbon or dopant atoms (B, N, Si) in graphene.[35]

The total displacement cross-section depends on the energy of the incident electron and the threshold energy (Figure 2b). With measurements on different carbon isotopes,[26,36] we have highly reliable values of the displacement threshold in graphene (Figure 2c). By changing the mass of the atoms and keeping the irradiation parameters constant, direct access to the ballistic displacement cross-section is possible. For graphene samples of the two isotopes C^{12} and C^{13}, the number of vacancies in a monolayer after a given irradiation dose has been measured. For C^{12} graphene, the onset of defect formation has been observed slightly above 80 keV (corresponding to $T = 21.1$ eV of the displaced atom). The displacement cross-section increases smoothly from zero at 80 keV to 0.2 barns at 100 keV and then rises steeply. For C^{13} graphene, the same behavior appears at electron energies that are ≈10 keV higher. Although thermal atom vibrations alone do not lead to defects, atomic vibrations have to be considered when the threshold energies are calculated.[23,36,37] It has been found that electrons of <100 keV can't displace carbon atoms in graphene without additional temperature effects. The momentum of the vibrating atoms has to be added to (or subtracted from) the momentum transfer in a ballistic collision.

In graphene or graphitic nanoparticles, the displacement threshold is highly anisotropic and has been studied by first-principles and molecular dynamics simulations.[37,38] As expected, the out-of-plane displacement threshold is much lower than the in-plane value. When the electron beam is parallel to the graphene layer, large scattering angles are needed to finally lead to out-of-plane displacements because there is no space for in-plane interstitials in graphene. Values have also been measured for impurity atoms such as nitrogen on substitutional sites or as adatoms on graphene.[37]

Irradiation may lead to defects in graphene even when no vacancy-interstitial pairs are created. An example is the Stone–Thrower–Wales defect[39,40] where a carbon-carbon bond in graphene is rotated by 90°. This transforms four hexagons into two adjacent heptagons and two separated pentagons. This defect doesn't involve the ejection of atoms and requires slightly less energetic electrons[41] than for the formation of vacancies (atoms are displaced when a Stone–Thrower–Wales defect is created but remains in the layer).[42]

Carbon atoms sitting at the edge of a graphene layer are undercoordinated or saturated with foreign atoms (e.g., hydrogen). Due to the weaker bonding of edge atoms, the displacement threshold is lower than for atoms within the layer. A value of 14.1 eV has been determined experimentally.[43] Carbon atoms at armchair edges seem to be more stable under irradiation than at zigzag edges.[44,45] An earlier study, however, indicated the opposite.[46] The easy displacement of edge atoms is a frequent hindrance in TEM studies of graphene, even below an acceleration voltage of 80 kV, because there are often open edges or little holes in the layer so that only highly perfect layers withstand the irradiation. Another obstacle is the residual gas pressure in the microscope column or contamination (quite common on graphene) that might be ionized under the beam and react with the layer.

© 2024 The Authors. Small published by Wiley-VCH GmbH

It has been observed that holes in graphene grow at acceleration voltages of 60 kV and that the growth speed increases with increasing residual gas pressure.[47] Even secondary displacements may happen, where momentum is transferred by a beam electron to a hydrogen atom on the surface, which, on its part, may transfer sufficient momentum onto a carbon atom in graphene to create a vacancy.

With the focused beam in a STEM, the displacement of preselected atoms in graphene is possible[17,35] but has its limitations. It is of interest for studying the behavior of dopant atoms on substitutional positions. The displacement thresholds of dopant atoms are different from those of carbon due to their different mass and the generally weaker bonding of the dopant within the graphene lattice. For example, whereas a threshold of 21.1 eV has been measured for the displaced carbon atom in graphene,[36] the threshold for a substitutional boron atom is only 15.9 eV.[48] A review of the different experimental and theoretical values of threshold energies and displacement cross-sections is given by Susi et al.[35] The advantage of STEM is the possibility of identifying the dopant atoms and following their migration during the reconstruction around the defects. This is impossible in pure graphene because different carbon atoms can't be distinguished, short-lived transient atom configurations during the reconstruction can't be seen and it is difficult to follow the path of individual carbon atoms. Interesting new approaches of nanopatterning graphene with a focused electron beam in a STEM have been shown recently.[49–51] By using convolutional neuronal networks, new horizons of atom-scale structuring are coming into sight.

Displacement cross-sections and threshold energies in bulk graphite are slightly different from the values in graphene. This is mainly due to the different bonding in graphite where the interstitials can serve as bridges between neighboring layers so that the inter-layer migration of interstitials is slower than the migration of adatoms on the surface of graphene.[52,53] Since the observation of individual vacancies by TEM in graphite (or in multiwall carbon nanotubes or few-layer graphene) is more difficult than in graphene, no precise values for the displacement threshold are available yet. Values obtained by other techniques over decades range from 10 to 70 eV. Recent molecular dynamics simulations indicate a threshold of 22 eV[28] which is only slightly higher than the value of graphene.

Graphene layers have already been used to wrap other materials and so to reduce radiation damage in different species. Damage in MoS_2 layers is efficiently suppressed when the MoS_2 layers are sandwiched between graphene layers.[54,55] This phenomenon can also be made use of when radiation-sensitive molecules are encapsulated in graphitic shells.[56] The reduction of open space by outer layers prevents the ejection of atoms.

4. Radiation Defects

We will concentrate here on radiation-induced point defects in graphene and nanoparticles based on the graphene lattice such as carbon nanotubes. Detailed reviews about defects in graphene have already been published earlier,[19,57] therefore, we will just summarize what is of importance in the context of irradiation. Extended defects (dislocation-like defects, domain boundaries, etc.) will not be the subject of this review.

The interest in graphite as a moderator for nuclear reactors motivated research on radiation defects in graphite since the 1960s. However, early work about vacancies or interstitials in graphite[58] had to be revised after the discovery of reconstruction effects around vacancies and different bonding configurations of interstitials. The configuration of vacancies and interstitials in graphene or graphite is surprisingly diverse in comparison to simple bulk crystals, where a vacancy is just a missing atom and interstitials are localized on or moving between sites of high symmetry (e.g., tetrahedral or octahedral sites in cubic crystals). Removing carbon atoms leads to a local reconstruction of the initially hexagonal network, and interstitials may be in different configurations between the layers in graphite or as adatoms above the layer in graphene.[59] While the configuration of vacancies is easily visible in TEM images, interstitial atoms are still difficult to detect due to their rapid migration and their projected overlap with the graphene or graphite lattice. Our knowledge about interstitials in graphene and nanotubes still depends on indirect experimental evidence and on calculations.

4.1. The Stone–Thrower–Wales Defect

As mentioned above, the Stone–Thrower–Wales (STW) defect is created by the rotation of a single carbon-carbon bond by 90° in the graphene lattice and does not involve the removal of atoms.[39,40] Four neighboring hexagons are converted to two pentagons and two heptagons (**Figures 3**,**4**), and the defect is usually denoted as STW(55-77). The formation energy of an STW defect is ≈5 eV[60,61] and therefore lower than the formation energy of a single vacancy (7.4 eV).[31] The kinetic barrier for the STW formation is ≈10 eV and much higher than its formation energy, whereas the barrier for the relaxation back to the perfect lattice is only 5 eV.[61] No carbon atom is undercoordinated, but the broken symmetry in the graphene lattice leads to local strain. Due to the lower formation energy of STW defects, a structural disorder in the graphene lattice already appears at electron energies slightly below the threshold energy for vacancy formation.[42] The STW defect may also play a role in the reconstruction of the lattice after the formation of one or several single vacancies. The accumulation of STW defects under sustained irradiation leads to a graphene lattice with a high concentration of pentagons and heptagons and eventually to a quasi-amorphous 2D network.[62]

4.2. Vacancies

Vacancies in graphene can easily be seen in aberration-corrected electron microscopes. The advantage of in situ TEM is that the formation of vacancies by electron irradiation can be monitored in real-time. A single vacancy is formed by the removal of a carbon atom from the graphene lattice.[63] Two of the dangling bonds from the three neighbor atoms may close so that one open bond remains. The lattice around the single vacancy is a combination of a nine-membered and a five-membered ring (Figure 4); this is denoted as a V_1(9-5)-defect. Due to the unfavorable dangling bond, the single vacancy is energetically high (7.5 eV), and the vacancy tends to coalesce with other vacancies (see below).

The migration of single vacancies is still not fully understood. Calculations reveal a rather low migration barrier of 1.3 eV;[31,65]

© 2024 The Authors. Small published by Wiley-VCH GmbH

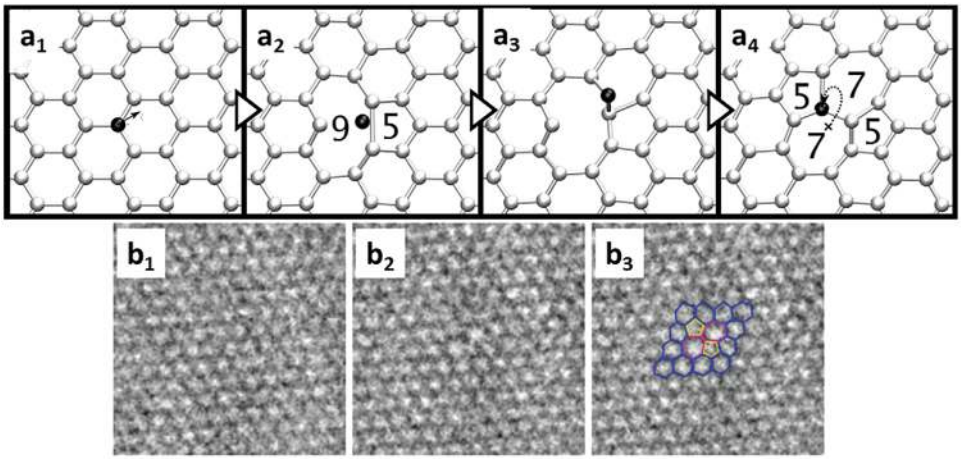

Figure 3. Model a) and TEM images b) of a Stone–Thrower–Wales defect.[42] a_1): A carbon atom is displaced upwards; a_2): a pentagon and a nonagon are formed while the adatom moves over the layer; a_3): the adatom bonds to a carbon atom of the pentagon; a_4): the adatom jumps back into the layer so that two heptagons and two pentagons are left. The TEM images b) show the pristine graphene lattice b_1) and the STW defect b_2, b_3). Courtesy J. Kotakoski, reproduced with permission, copyright 2011 American Physical Society.

this would make single vacancies mobile above 200–300 °C.[66] It should be possible to monitor such a migration in lattice images at elevated specimen temperatures, but this has not been reported to date.[67] An in situ annealing of radiation damage in graphitic nanoparticles (tubes, onions) at elevated specimen temperatures has been observed indeed in early studies[68,69] (see Section 4.4), but it was just the absence of extended defects under irradiation that has been noticed, and no atomic picture was possible at that time.

Energetically more favorable defects in the graphene lattice are divacancies. As shown in Figure 4, the lattice can fully reconstruct around a divacancy without dangling bonds. Divacancies are formed when two neighboring carbon atoms are removed or when two single vacancies coalesce. The simplest divacancy is the combination of two pentagons and an octagon V_2(5-8-5), but other configurations such as three pentagons and three heptagons V_2(555-777) or four pentagons and four heptagons around a central hexagon V_2(5555-6-7777) are also possible (Figure 4). The formation energy of a divacancy is only 8 eV[31,65] and much lower than twice the formation energy of a single vacancy (2 × 7.5 eV). On the other hand, the activation energy for the migration of a divacancy is 7 eV,[31] making it immobile up to very high temperatures (however, under irradiation, restructuring leading to a lateral displacement is possible).[32] Geometric considerations show that multiple vacancies with an even number of missing atoms reconstruct without dangling bonds which makes them energetically favorable against odd-numbered vacancies. Many different irradiation-induced vacancy configurations have meanwhile been detected in TEM studies of graphene.[42,62,70–77]

4.3. Interstitials and Ad-Atoms

While interstitial atoms in multi-layer graphitic structures are located between the layers (there is no potential minimum for extra atoms within the densely-packed layers),[52,53,78] we consider interstitials on monolayer graphene as adatoms. In early studies, it has been assumed that interstitials in graphite are located between the layers without interacting with them.[58] This would lead to an extremely low migration barrier (<0.1 eV) which is not compatible with the observed annealing effects. Later, it was realized that interstitials form bonds with their neighboring layers, and several bonding configurations of interstitials or adatoms have been studied in simulations.[52,53,78,79]

Bonding between the interstitial and the perfect or defective graphene lattice (we assume that no dangling bonds prevail) needs the re-hybridization of an atom within the layer toward sp^3 (in a simplified picture, four bonds are needed to close three bonds in the layer and to attach the interstitial). The interstitial can be located in different positions above the layer (**Figure 5a**);[79,80] the most favorable is the bridge position above the edge of a hexagon with a binding energy of 1.5 – 2 eV.[81,82] A migration barrier for adatoms on graphene of 0.4 eV has been calculated[82] which is much lower than for vacancies and makes adatoms mobile at room temperature. Due to their rapid migration, they should be invisible in TEM images. In graphene or graphite,[79,83] interstitials may also appear in a dumbbell configuration where the adatom pushes an atom of the layer toward the opposite side so that a symmetric configuration with one atom above and one below the layer is created (Figure 5a,b). With a migration barrier of the dumbbell of 0.9 eV, it is less mobile than a bridge adatom. The interstitial atom in graphite can be located in the middle between two layers (Figure 5b,c) and form bonds with each of them.[59,61,79,83] Such a sp^3-hybridized interstitial in a spiro configuration (Figure 5b) should be less mobile than in the other configurations. Similar configurations as in graphene appear when the interstitial is in the grafted or dumbbell configuration. An interesting situation appears when a dimer of interstitials is formed.[84,85] It can be integrated into the graphene layer (Figure 5a) by creating an inverse Stone–Thrower–Wales (ISTW) defect I_2(7557). The ISTW defect is different from the STW defect in that the two pentagons instead of the two heptagons join. The ISTW defect changes the local curvature of the lattice so that

© 2024 The Authors. Small published by Wiley-VCH GmbH

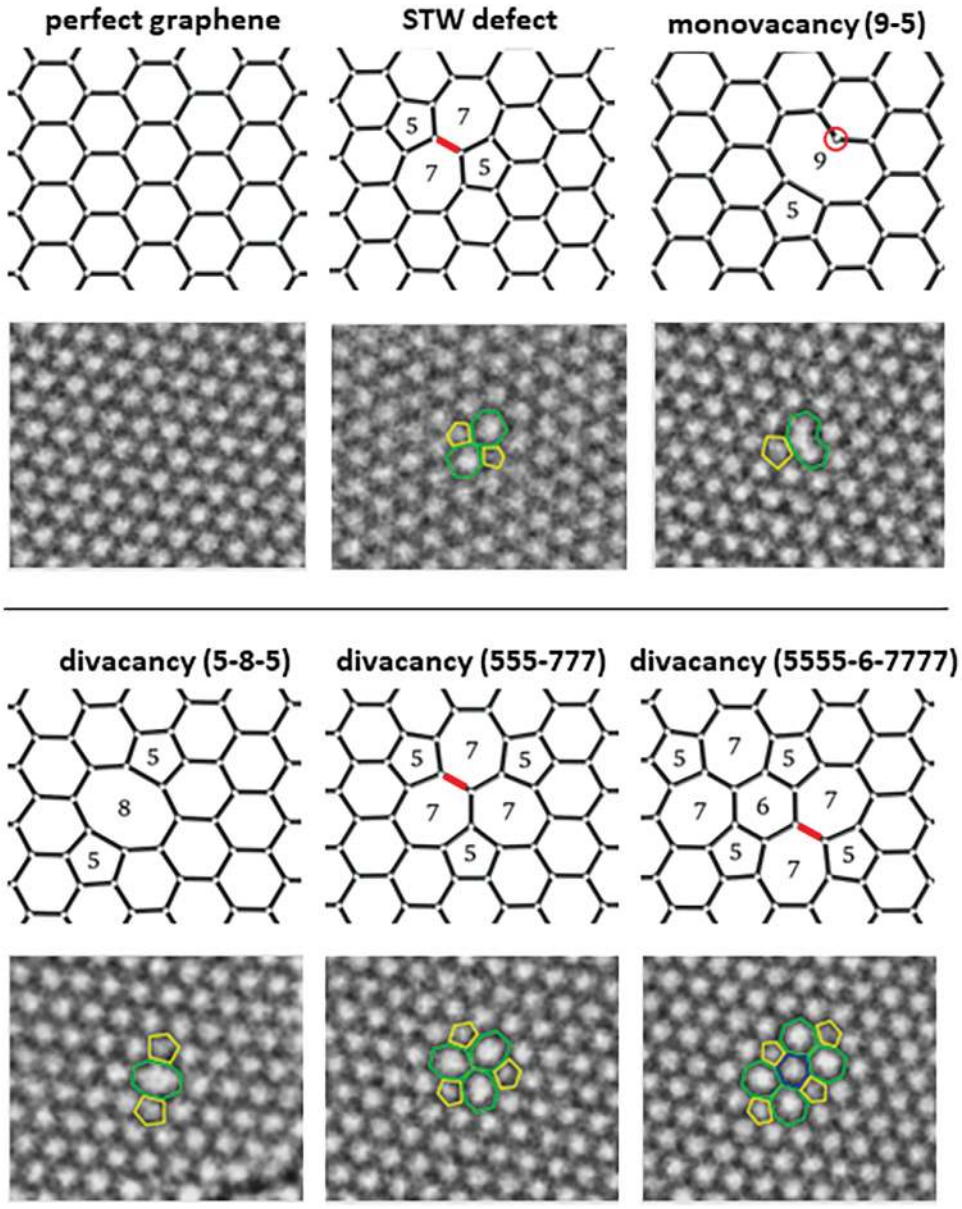

Figure 4. Models and TEM images of perfect graphene, the STW defect (two pentagons and one heptagon), a monovacancy (one pentagon and one nonagon), and different types of divacancies, composed of pentagons, hexagons, heptagons, or octagons.[62,64] Courtesy A. Krasheninnikov and J. Kotakoski, reproduced with permission, copyright 2011 American Physical Society.

a hillock is formed. In graphite, double interstitials in different configurations may appear (Figure 5c).[79]

The penetration of interstitials through the hexagons of a perfect graphene layer is not possible due to the high kinetic barrier. However, the penetration of even large foreign atoms through vacancies in single-wall carbon nanotubes has already been observed.[86] Therefore, in the presence of vacancies, atom migration normal to the layers of graphene or graphite seems to be possible. The penetration of adatoms though perfect graphene might be possible through the dumbbell configuration,[79,83] where the adatom exchanges its position with atoms in the layers. This could allow an efficient diffusion of adatoms perpendicular to the layers in a graphitic structure. An energy barrier of 1.2 – 1.7 eV for the migration of interstitials perpendicular to the layers has been calculated[83] which would allow transport along the c-axis of graphite at elevated but still moderate temperatures.

4.4. In Situ annealing

It has already been observed in the 1990s that carbon nanotubes and graphitic onion-like particles are much more stable under the electron beam in the TEM when the specimen is held at temperatures above 200 – 300 °C.[68,69] This has been confirmed in several later studies.[88,89] Under room temperature irradiation,

© 2024 The Authors. Small published by Wiley-VCH GmbH

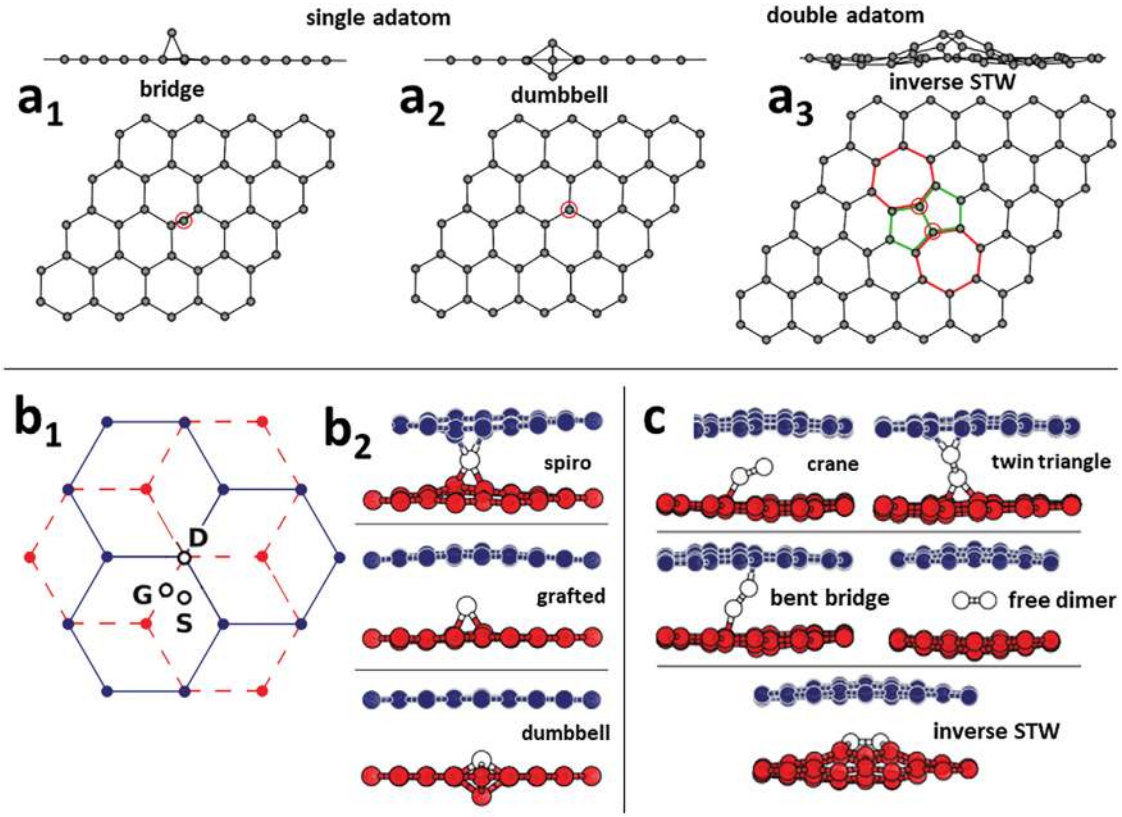

Figure 5. Adatoms on graphene a) and interstitials in graphite b,c).[19] Single adatoms on graphene are shown in the bridge a_1) and the dumbbell a_2) position and a double adatom forming the inverse Stone–Thrower–Wales defect a_3). Single interstitials in graphite b) are shown in the spiro, grafted, and dumbbell configuration in top-view b_1) and side-view b_2). Double interstitials are shown in the crane, twin triangle, bent bridge, free dimer, and inverse STW configuration c).[79] Courtesy A. Krasheninnikov, reproduced with permission, copyright 2011 American Physical Society.

the rupture of graphenic planes appears and leads to ongoing disorder in the graphitic lattice (see Figure 8 in Section 5.3). The in situ annealing was tentatively explained by an increased mobility of defects, but the nature of the migrating defects remained, for the time being, unclear. Later, it was observed that if the accumulated defects were already present after room-temperature irradiation, much higher temperatures, approaching 1000 °C, were necessary to anneal the lattice.[90–92] The phenomenon was taken up again when the influence of lattice vibrations on the displacement threshold was studied.[23,36,37] Due to increased atom vibrations, irradiation at higher temperatures should even lead to an increased defect formation rate, which is observed at the atomic scale but is not in accordance with the observed in situ annealing effect. Therefore, an efficient annealing mechanism, where the migration barrier of the defect is ≈1 eV, could explain the phenomenon.

Since adatoms in the bridge position have a migration barrier of 0.4 eV, their high mobility should already lead to efficient annealing at room temperature which is, however, not observed. Single vacancies with a migration energy of 1.4 eV would explain the annealing, but, as stated above, their migration has not been observable in high-resolution TEM studies at elevated specimen temperatures.[67] In an indirect measurement, the migration barrier of defects healing radiation damage in graphene at a known defect production rate has been studied, and it has been stated again that adatoms with a migration barrier of 0.33 eV could explain the annealing in monolayer graphene.[67] However, most of the previous experiments were carried out on multi-layer graphitic structures where more strongly bound interstitials[61,79,83] with higher migration barriers could be responsible for the in situ annealing. It has to be emphasized that the threshold temperature for in situ annealing always seems to be in the same range (≈300 °C), irrespective of the dose rate and the presence or absence of carbon or hydrocarbon contamination that could act as a source for interstitial atoms. Hence, the annealing problem is still not completely solved today, although realistic scenarios (single vacancy migration, inter-layer interstitial migration) could serve as an explanation, though not without some contradictions.

5. Collective Radiation Effects: Topology Changes and New Structures

5.1. Irradiation Phenomena in Carbon Nanotubes

Many electron irradiation studies of carbon nanotubes have been carried out from the beginning of the nanotube era in the 1990s[93–95] until today,[96] too numerous to refer to all of them here. Carbon nanotubes are based on the graphene or graphite lattice, so the configurations of point defects are thought to be

© 2024 The Authors. Small published by Wiley-VCH GmbH

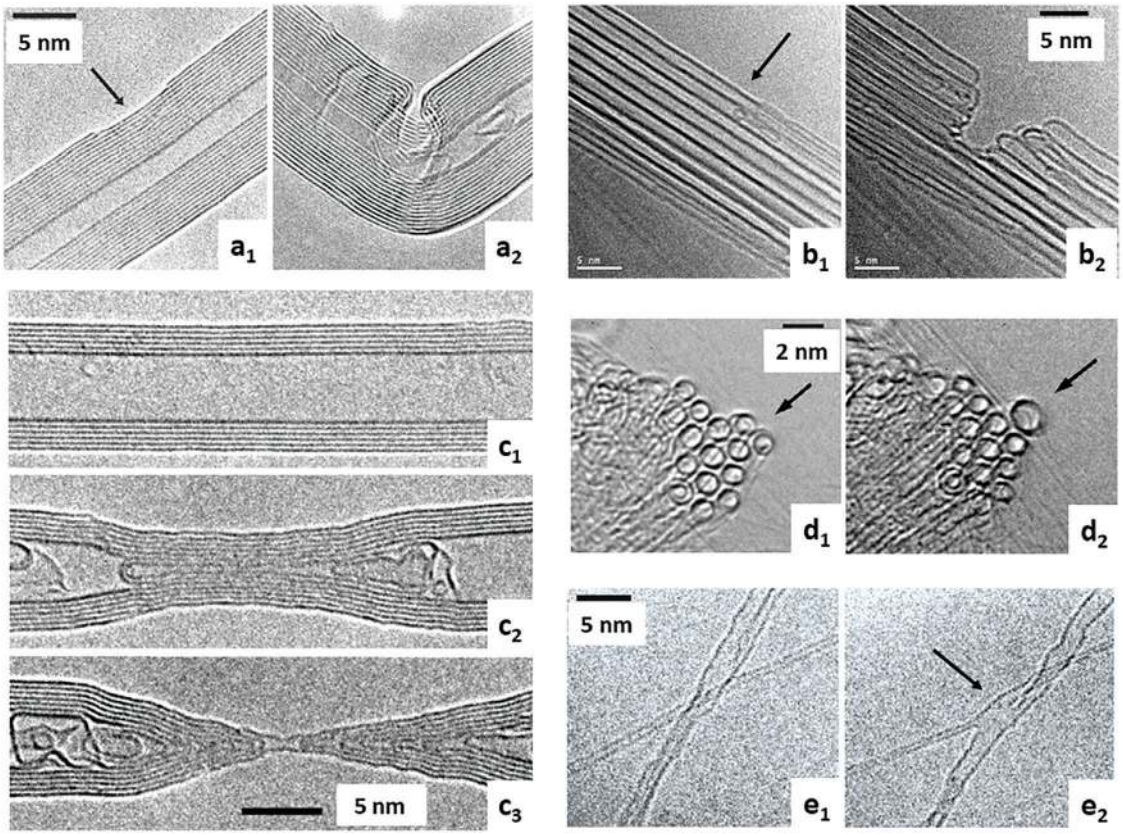

Figure 6. A selection of electron irradiation phenomena observed in studies of carbon nanotubes. The specimen temperature was mostly in the range of 500–700 °C and thus always above the in situ annealing temperature. a) Multi-wall nanotube exposed to an electron beam focused onto a 5 nm spot on one side of the nanotube; a_1): at the beginning of irradiation; a_2): the irradiated side shrinks after irradiation, leading to bending of the tube.[105] b): Bundle of single-wall nanotubes irradiated with an electron spot of 5 nm; b_1): before irradiation; b_2): after irradiation. The tubes have closed their ends when cut by the beam.[106] c): Collapse of a multi-wall tube under an electron beam spot of 20 nm. The sequence shows the shrinkage of the tube and the transformation into a single-wall tube in the center of the beam.[107] d):The coalescence of parallel single-wall tubes within a bundle under electron irradiation viewed in cross-section.[108] e): The coalescence of crossing single-wall nanotubes under electron irradiation.[109]

the same as in single-layer graphene or multi-layer graphite. In most of the experiments, nanotubes have been irradiated at room-temperature where the agglomeration of immobile defects[58] leads to a rupture of the layers, as has already been observed in bulk graphite samples.[97] Eventually, this leads to the destruction of the tube. The interrupted planes have sometimes been described as "dislocations" because of their appearance in the projection, resembling drawings of edge dislocations viewed end-on. However, this concept is misleading because the ruptures appear everywhere, and the dislocation core would have to be curved all around the tube, which is not observed. It is surprising how often the same phenomenon has been described again, but this could be due to the fact that the destruction of the tubes under the beam is inevitable and very conspicuous in every study of nanotubes at 200 – 300 kV where common TEMs are operated.

The interrupted layers after irradiation act as covalent inter-shell links that prevent sliding of the shells inside each other and lead to a stiffening of the tubes.[98] With a focused electron beam, nanotubes have been punctured;[99] this may even lead to a release of gas that is stored inside the tubes.[100]

Carbon nanotubes show more interesting effects when the irradiation is carried out above the in situ annealing temperature of 300 °C (**Figure 6**). The threshold energy for atom displacements depends on the irradiation direction relative to the local orientation of the curved lattice.[94] With a beam orientation in c-direction (perpendicular to the surface), a minimum value of 86 keV has been determined.[101] This is close to the threshold of graphene.[23] However, the stability of single-wall tubes under irradiation increases with the diameter of the tubes.[102] High cylindrical curvature causes an increase of the sp^3 character of the bonds which is energetically less favorable than a flat graphene layer and leads to surface tension. The lower bonding energy of each carbon atom is thus reflected by the higher displacement rate. A striking example of this phenomenon is the coalescence of fullerene molecules inside single-wall nanotubes ("peapods").[103,104] The threshold energy for the transformation of the C_{60} molecules, which have a large curvature and a sp^3 character of 10%, is lower than for the tubes so that the tube remains undamaged at 80 keV while the fullerenes coalesce.

Nanotubes shrink due to the loss of atoms (Figure 6c)[110] and, just as carbon onions, exert pressure on materials that they encapsulate.[111,112] Local shrinkage of the tubes, e.g., under a

© 2024 The Authors. Small published by Wiley-VCH GmbH

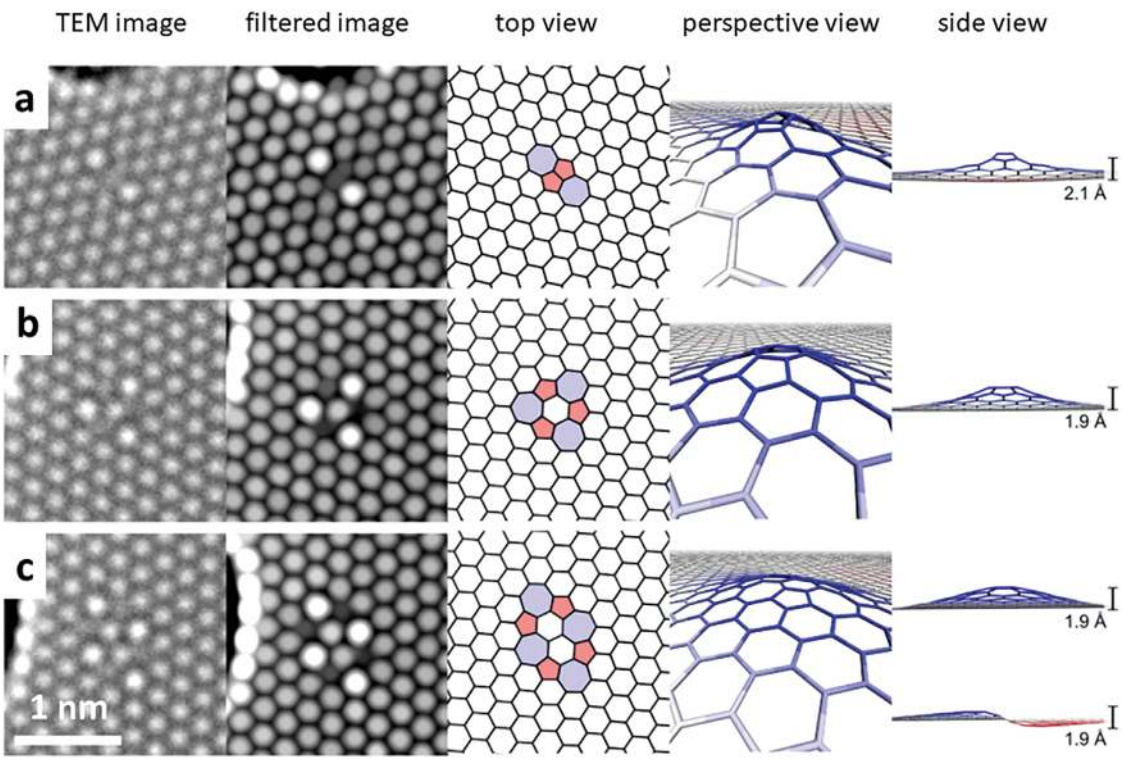

Figure 7. Curvature of a graphene layer by the integration of interstitials. a): An inverse Stone–Thrower–Wales defect as an interstitial dimer; b): the interstitial dimer after one bond rotation; c) after two bond rotations.[76] Courtesy U. Kaiser, reprinted with permission from O. Lehtinen et al., Nano Lett. **2015**, *15*, 235, copyright 2015 American Chemical Society.

focused electron beam, leads to constriction in an hour-glass shape[110] where the surface locally exhibits negative curvature and the presence of heptagons. Single-wall nanotubes within a bundle coalesce under irradiation Figure 6d)[108] so that larger tubes are formed. The increasing diameter reduces curvature and thus the energy of the tube. Crossing single-wall tubes may join under irradiation and form molecular junctions (Figure 6e).[109] Carbon nanotubes can serve as channels for the diffusion of interstitial atoms. The open space inside the tube acts like a surface in graphene. By cutting single-wall carbon nanotubes repeatedly with an electron beam (Figure 6b) at different separations between the cuts and by measuring the cutting speed, an indirect value for the migration energy of interstitials inside the tube of 0.25 eV has been obtained.[106] It has also been shown that vacancies or larger holes can be created in single- or multi-wall carbon nanotubes with a focused Ångstrom-size electron spot in a STEM.[99,113]

5.2. Defect-Mediated Curvature of Layers

Since the first models of the bonding geometry of fullerenes were shown,[1] it became clear that the Gaussian curvature of a graphene sheet in two directions needs the presence of pentagons or heptagons. Cages such as the fullerene C_{60} need 12 pentagonal rings to ensure spherical closure without dangling bonds. The same holds for faceted onion-like graphitic nanoparticles where the pentagons are localized at the tips.[114,115] Pentagons lead to positive (spherical) curvature while heptagons lead to negative (saddle-like) curvature of the layer. By combining pentagons and heptagons, interesting architectures with a large variety of topologies are possible.[8,9,116]

Vacancy defects including pentagons and heptagons locally warp the graphene lattice; however, the curvature in symmetric defects in the 5–7 configurations such as the divacancy V_2(555-777) do not lead to an overall curvature of the structure. On the other hand, non-symmetric configurations such as the inverse Stone–Thrower–Wales defect I_2(7557)[76,85] lead to curvature (**Figure 7**). If the integration of an interstitial dimer into the graphene lattice by forming an inverse STW defect happens repeatedly, e.g., under irradiation where interstitials are always created, a curvature of the whole graphene sheet should appear.

A high number of extra carbon atoms leads to the formation of dislocation dipoles with curvature upwards and downwards.[76] However, this is only favorable in single-layer graphene where there is space for curvature on both sides. If we imagine different directions of curvature in a dislocation-like defect or in different defects (i.e., one is curved upwards and the other downwards) in multi-layer graphene or graphite, this would lead to an unfavorable increase of the interlayer distance beyond the van der Waals distance. However, the inter-layer distance can be maintained if all defects are of the inverse STW type and lead to the same curvature, i.e., a common curvature in one direction, eventually resulting in an overall spherical shape of the whole graphitic structure.

© 2024 The Authors. Small published by Wiley-VCH GmbH

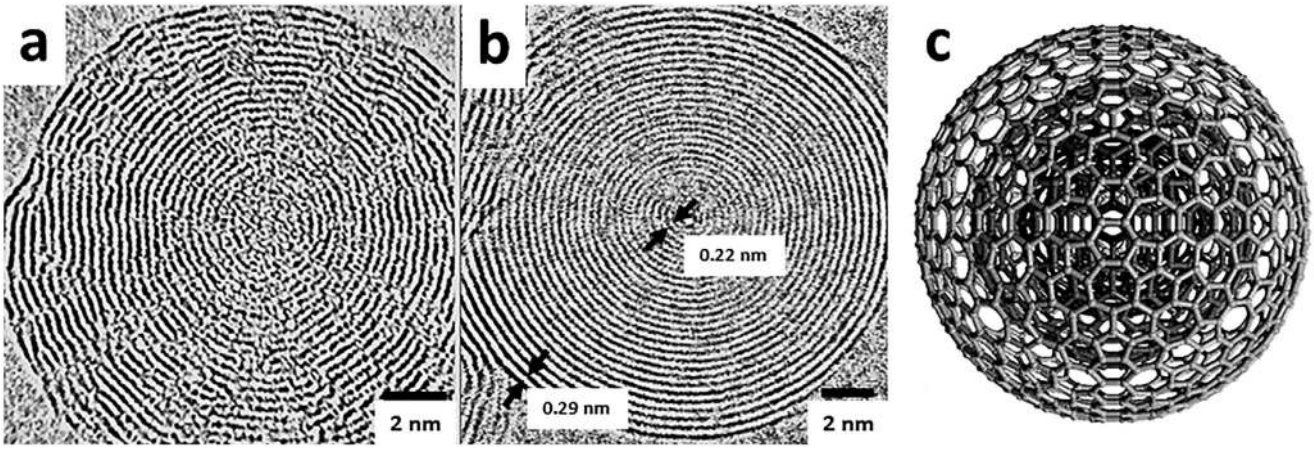

Figure 8. Spherical onion-like particles generated by electron irradiation of polyhedral graphitic particles.[68,87] a): Irradiation at room temperature leads to a defective structure. b): Irradiation at 700 °C leads to a coherent lattice and the self-compression of the particles (inter-shell spacings are indicated). c) Model of a multi-shell carbon onion built up of pentagonal, hexagonal, and heptagonal rings[8] (courtesy M. Terrones).

Such a curvature of graphitic particles under electron irradiation has been observed in the formation of spherically closed carbon onions.[10]

5.3. The Formation of Spherical Particles

The closed onion-like structure (**Figure 8**) is energetically favorable because dangling bonds are avoided all over the particle. In larger cages than the fullerenes, the presence of 12 pentagons leads to a faceted cage[117] where the facets are flat and the pentagons are at the tips of the polyhedron. However, a suitable combination of pentagons and heptagons may lead to larger cages with perfectly spherical shapes as structure calculations have shown (Figure 8c).[8,118] Although it was not possible to reveal the defect arrangement in carbon onions experimentally, nested graphitic cages containing pentagons and heptagons remained the best model to describe the structure.

Irradiation of graphitic structures leads to the continuous generation of interstitials that migrate and join so that interstitial dimers are created. The dimers can be integrated into the layers via the inverse STW mechanism. Bond rotations may lead to similar defect combinations with local curvature.[76] If all of the resulting hillocks are on the same side of the layers, this leads to curvature of the layers by maintaining the van der Waals distance between the layers. The formation of carbon onions under electron irradiation can therefore be explained by a collective effect of defect generation that leads to the formation of a self-organized structure. The process in itself is striking because a more or less disordered graphitic aggregate can be transformed into an arrangement of spherical graphitic balls just by bombarding it with energetic electrons.[10,69,119] This is a highly dissipative process under far-from-equilibrium conditions but leads to structure formation nevertheless.

Performing the irradiation at temperatures above ≈300 °C ensures sufficient mobility of interstitials and/or monovacancies and thus a coherent lattice within the shells (Figure 8b). Under these conditions, a self-compression effect has been observed,[68,69] reducing the spacing between the shells from the equilibrium value of graphite (3.3 Å) on the surface to ≈2.2 Å in the center. Qualitative models are based on the removal of atoms from the shells that lead, upon closure, to smaller shells. The loss of atoms from the outermost shells leads to pressure inside the particle. Interstitial atoms may penetrate the layers, e.g., by the dumbbell mechanism or the exchange of inter-layer interstitials,[60,61,79,83] so that a radial migration of atoms is possible, though at a low rate. With a migration barrier along the c-direction in graphite of 1.2 – 1.7 eV,[83] the transport of carbon atoms in the radial direction should be possible at elevated temperatures. The pressure gradient in the onions leads to a preferential migration of interstitials outwards so that all shells exert pressure toward the center. After extended irradiation, the heavy self-compression can lead to a phase transformation and the nucleation of diamond crystals in the center of the onions.[68] A quantitative calculation using rate equations based on radial point defect migration describes the self-compression and buildup of pressure.[120] An alternative mechanism involving the radial migration of dislocation-like defects has been suggested.[121] Carbon onions have shown to be versatile capsules to enclose crystalline materials such as metals,[122,123] and many interesting experiments, making use of compressive action of the graphitic shells under irradiation, have been demonstrated.[124,125]

6. Irradiation-Induced Shift of the Graphite-Diamond Equilibrium

After the discovery of diamond nucleation in the center of carbon onions, it has been observed that the diamond nuclei in the onions grow under sustained electron irradiation.[87,126] Later, this experiment was repeated on planar graphite-diamond interfaces where the diamond phase grew at the expense of graphite at temperatures above ≈300 °C[127] but in the absence of pressure (**Figure 9a–c**). This was against all expectations because electron irradiation should lead to the reverse and transfer the activation energy to transform the metastable diamond phase into the energetically lower graphite phase. The transformation of

© 2024 The Authors. Small published by Wiley-VCH GmbH

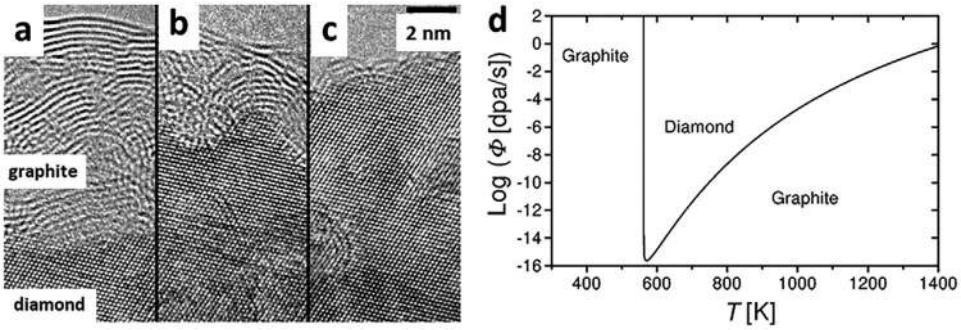

Figure 9. Transformation of graphite to diamond under electron irradiation. a – c): Electron irradiation of a graphite-diamond interface at 700 °C leads to the growth of diamond at the expense of graphite, visible as the migration of the interface upwards from a) to c).[127] b): Calculated phase diagram showing the stability of the respective phases as a function of the atom displacement rate Φ (in displacements per atom and second) and the temperature *T*.[130,131]

diamond to graphite has already been observed when diamond nanocrystals were transformed into onion-like particles by heat treatment[128] or under electron irradiation.[129] The phase transformation from graphite to diamond under electron irradiation was then explained by a quantitative model based on the different displacement cross-sections in graphite and diamond.[130,131] The theory uses a master equation formalism to calculate the probability of finding an atom in one or the other phase and considers the two opposing driving forces at the interface between graphite and diamond. Thermal effects drive the system to the more stable graphite phase so that a transformation under equilibrium conditions would lead to the growth of graphite. However, the atom displacement rate under electron irradiation is much higher in graphite than in diamond so mobile atoms at the interface that attach to the diamond crystal survive there for a longer time than those attached to the graphite crystal. So, in a suitable range of temperatures and irradiation intensities, the diamond appears indeed as the more stable phase and may grow under these conditions. A non-equilibrium phase diagram (Figure 9d) was calculated to show the stability of the two phases as a function of the displacement rate (dpa s^{-1}) and the temperature.[130] This is another example of a dissipative system where a highly ordered system (an almost perfect diamond crystal) grows at the expense of a rather disordered system (defective graphite) under non-equilibrium conditions. Naively, one would expect that the bombardment with energetic electrons leads to an increase of entropy and to a more disordered phase which is quite obviously not the case at the graphite – diamond interface.

7. Linear sp^1 Carbon Nanomaterials

Chains of carbon atoms in the sp^1 bonding configuration[132,133] can be considered real 1D carbon structures because they have a monoatomic thickness in the two dimensions normal to the direction of the chain (carbon nanotubes have a non-zero radius and are 3D structures). The existence of bulk materials consisting of sp^1 carbon chains is still disputed. The chains are highly reactive and tend to form cross-links with neighboring chains and relax to the energetically lower graphitic sp^2 structure. However, isolated chains, where the reactive ends are saturated by other species or metallic contacts, are stable and have been observed in TEM studies. Point defects in a carbon chain do not exist because a vacancy would separate the chain into two halves. Irradiating the chains with electrons leads to their rupture. Adatoms might diffuse along the chains, but this hasn't been observed yet.

Nevertheless, carbon chains are of interest in the context of irradiation because they can be formed by the irradiation of carbon nanotubes or graphene with energetic electrons. The constriction of single-wall or few-wall carbon nanotubes has been observed in the focus of an electron beam (as shown in Figure 6c), and the hour-glass structure finally separates the two cones by leaving a chain of atoms for a short time until breakage occurs.[134] A similar phenomenon has been observed under irradiation of graphene layers where holes were formed by the loss of atoms. A chain appeared at the border between two growing holes before the holes joined (**Figure 10**b).[135,136] Both experiments have in common that the chains were more stable under the beam than their precursor (nanotubes or graphene), otherwise, they would not have formed. Unlike graphene with an unsaturated edge, chains have no dangling bonds so their stability is higher than that of atoms at the edge of a graphene layer or in narrow graphene ribbons.[44,135] It would be a simple experiment to measure the atom displacement rate in carbon chains under given irradiation conditions because the first atom displacement leads to the easily visible rupture of the chain. Qualitatively, this has already been observed at 200 keV;[135–138] however, the quantitative analysis hasn't been carried out yet. The threshold energy could also be determined, though with some difficulties. This would be an interesting value in view of the mechanical stability of the chains. Calculations predict that the mechanical strength of carbon chains is exceptionally high.[139] A comparison with the threshold and displacement rate in graphene would provide precious knowledge about the mechanical properties of sp^1 bonded carbon materials.

Electron irradiation also aided the formation of carbon chains between a metal tip and a graphenic aggregate (Figure 10a). By applying such a procedure with an STM tip that was integrated into a TEM specimen stage, the electrical properties of carbon chains have been measured (Figure 10d).[137] Indications for a metal-semiconductor transition have been found when strain was applied to the chain so that the transition between cumulene (only double carbon-carbon bonds) and polyyne (alternating single and triple bonds) occurred (Figure 10c).[140]

© 2024 The Authors. Small published by Wiley-VCH GmbH

8. In Situ Growth of Carbon Nanoparticles under Electron Irradiation

Catalytically active transition metals serve as seeds for the growth of carbon nanotubes or graphene.[141,142] The growth mechanism has been explained by the rapid diffusion of carbon atoms on the surface or through the bulk of the metal and the nucleation of a flat or curved graphitic network on the surface. The growth is normally carried out at high temperatures to ensure a high mobility of carbon atoms. Growth in a gaseous atmosphere can be monitored in situ in dedicated TEM reaction cells[15] but will not be reviewed here. Growth in the solid phase is more easily accessible to in situ observation because no special reaction cells are needed. For example, the growth of carbon nanotubes from polyyne-based solid precursors under electron irradiation has been monitored.[143] Electron irradiation has shown a considerable influence on the growth of nanotubes or graphene from metals in the solid phase. The mobility of carbon or metal atoms on the metal surfaces is increased by momentum transfer from the beam electrons. On the other hand, carbon atoms can be implanted into the metal when the energy transfer is high enough. Furthermore, the reaction barrier in the chemical interaction between catalytically active metal atoms and carbon atoms in the graphene network is overcome through momentum transfer by the energetic electrons. Using the same electron beam for irradiation and imaging allows the in situ monitoring of the growth of carbon nanoparticles in the TEM.

Before the observation of growth phenomena, it has been found that electron irradiation can be used to facilitate the formation of covalent bonds between carbon and metal atoms and so to create junctions between carbon nanotubes and metal particles. Experiments with a focused electron beam were carried out to weld single-wall nanotubes[144] or multi-wall nanotubes[145,146] to metal particles. The presence of metal atoms under electron irradiation has also shown etching effects in graphene[147] so that holes appear under the beam and grow while the metal atoms are migrating along the edges of the holes. The same mechanism has been observed in nanotubes[148] where metal atoms lead to the cutting of the tubes under the beam.

Multi-wall carbon nanotubes can be filled with transition metal cores by capillarity effects or in chemical vapor deposition,[93,149] and these composites turned out to be very versatile systems for studying the growth of nanotubes under electron irradiation. The irradiation of metal cores inside multi-wall tubes at high temperatures led to the growth of new multi-wall tubes from the end of the metal cores inside the host tubes.[150] The injection of carbon atoms into the metal and subsequent diffusion of carbon atoms through the bulk of the metal (the surface is covered by graphitic shells) appears to be a realistic scenario for explaining the growth.

Double junctions, where a metal particle separates two multi-wall tubes, were irradiated until the metal shrank to an hour glass shape. After the separation of the metal into two halves, a single-wall nanotube grew as a bridge between the metal cones (**Figure 11**a–c).[151] The growth of single-wall tubes was also observed on the surface of a metal particle terminating the end of a multi-wall tube. Again, the growth of the tubes is due to the diffusion of carbon through the metal or on the metal surface, and the whole process is driven by momentum transfer from the electron beam that aids in overcoming the kinetic barrier for the breaking and formation of bonds and for the diffusion of carbon atoms. Single-wall carbon nanotubes were also seen to grow inside boron nitride nanotubes attached to amorphous carbon substrates when they were subjected to electron irradiation.[152]

In situ experiments under electron irradiation have been carried out to observe the growth of graphene.[153] A transition metal layer on an amorphous carbon film was heated and irradiated with electrons. Irradiation caused the retraction of the metal film, leaving a graphene layer underneath (Figure 11d–f). It appears that carbon from the amorphous film has been implanted into the metal and segregated on the surface as a graphene layer. The irradiation is needed to move the metal layer; this is a phenomenon that has also been observed in other studies where metal particles were guided by a moving focused electron beam.[154,155] Graphene layers were also synthesized by electron irradiation of amorphous carbon layers on graphene or boron nitride substrates.[156] There are many more interesting irradiation phenomena in metal-carbon nanosystems but cannot be discussed all in the frame of this review.

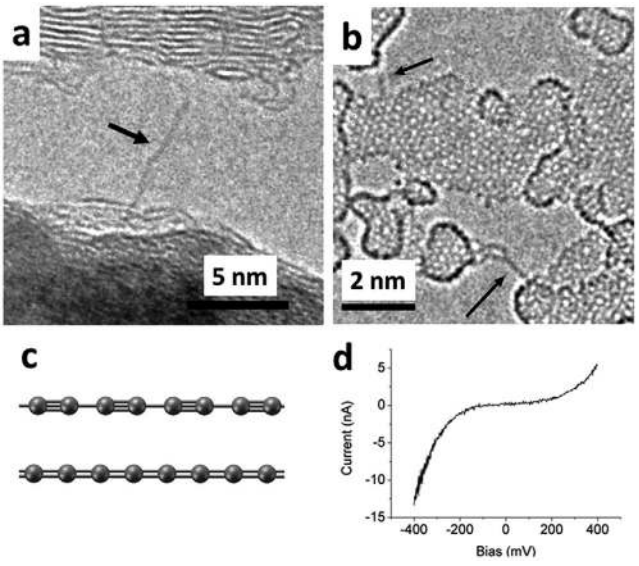

Figure 10. Chains of carbon atoms. a): A chain between a metal tip (bottom) and a graphitic aggregate (top).[137] b): Two chains (arrowed) created by electron irradiation of a graphene layer (courtesy U Kaiser, copyright IOP Publishing Ltd, and Deutsche Physikalische Gesellschaft. Reproduced by permission of IOP Publishing. CC BY-NC-SA).[136] c): Model of carbon chains in the polyyne (top) and cumulene (bottom) phase. d): Current–voltage characteristics of a carbon chain measured in a similar configuration as in a).[140] The curve shows the semiconducting behavior of the chain.

9. Conclusion

The irradiation of carbon nanoparticles based on the graphene or graphite lattice has shown a large variety of phenomena from the single-atom scale to the scale of hundreds of nanometers. The formation and dynamics of radiation defects such as vacancies or interstitials determine the properties and the morphology of the respective particles. Irradiation studies in the 1990s could only show morphological changes in graphitic particles, and the explanation of irradiation phenomena had to rely on models,

© 2024 The Authors. Small published by Wiley-VCH GmbH

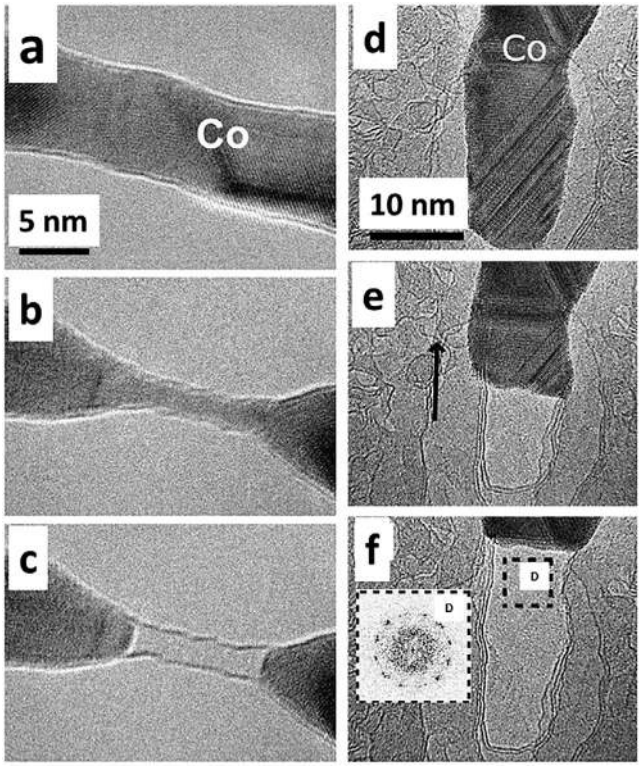

Figure 11. a–c): Growth of a single-wall carbon nanotube from a cobalt rod that is connected at its ends (not visible) to larger carbon nanotubes. After the thinning of the Co rod under electron irradiation b), the single-wall carbon nanotube appears between the ends of the separating Co tips c).[151] d – f): Growth of a graphene bilayer under the retracting end of a Co island on partly graphitized amorphous carbon. The diffractogram in f) was taken from the region marked with "D" and corresponds to a bilayer of graphene.[153]

sometimes based on outdated values of displacement threshold energies and formation or migration energies of different types of atomic defects. The situation changed immediately after the availability of aberration-corrected TEMs in the new millennium that allowed the imaging of every carbon atom around a defect. Another ground-breaking innovation was the synthesis of free-standing layers of graphene where the atomic lattice could, for the first time, be seen without any overlap. Single and multiple vacancies could be imaged and new computational studies provided more reliable quantitative data. With these innovations, many irradiation phenomena are now well understood. However, the field is still far from being concluded. Several questions remain, in particular concerning the configuration and dynamics of interstitials in the graphitic lattice or adatoms on the graphenic lattice that cannot be easily detected in TEM images. This is why several in situ annealing effects that have been observed since the 1990s are still not fully understood. So, there is enough space for future work.

What remains to be done?

We can say that the picture we have about different types of vacancies created by electron irradiation in the graphene lattice is complete. The high spatial resolution of modern TEMs and STEMs allowed the unequivocal identification of vacancies, and a further improvement of the image resolution will most likely not provide additional information. However, adatoms have not been identified clearly yet, and information about their position on the layer would be necessary to test the theoretical work of several decades. Adatoms are expected to migrate rapidly, even at room temperature, and pinning them at low temperatures by using a cooling stage in the TEM could possibly allow to detect them. Slowly raising the temperature could make the migration path of adatoms visible. Of particular interest would be the penetration of adatoms through the layer and the position of interlayer interstitials in graphite, but this could only be visible in a side-view geometry of the layers. This will be a very challenging project but could be possible by using carbon nanotubes where the projected periphery allows a view in the (curved) plane and to see an inter-layer exchange of atoms.[86]

Another task could be the monitoring of the migration of vacancies at high temperatures. Surprisingly, this hasn't been possible yet, but in a high-temperature stage that is stable enough at temperatures approaching 1000 °C, this could be feasible. The coalescence of single to double vacancies should be visible once the migration appears. An important innovation that could facilitate the visibility of the rapid migration of vacancies or interstitials is the availability of direct-detection CMOS cameras that allow monitoring in situ processes with higher frame rates and less image noise than conventional CCD cameras. Modern TEMs with lower acceleration voltages equipped with fast cameras should allow taking real-time movies of defect migration in graphene or nanotubes.

The structuring of graphene or nanotubes with a sub-Ångstrom beam in a STEM bears considerable potential, particularly when the beam-guiding system is controlled by machine-learning algorithms.[51] These techniques haven't by far been exhausted. Regular defect patterns or lateral superlattice structures could be created that change the electronic properties of graphene so that new applications can be envisaged. Catalytically active metal atoms on the surface or the presence of a reactive atmosphere can aid the structuring of graphenic layers under electron irradiation,[157] in particular when a wide temperature range is accessible.

The complementarity of electron microscopy studies and computational simulations will remain important. We have seen that the spatial resolution of modern TEMs is sufficient for seeing all details of defect arrangements, e.g., in monolayer graphene. However, the temporal resolution of TEMs is far from allowing us to follow the fast atom dynamics during the displacement process. This underlines the importance of simulation studies that cover timescales from femto- to nanoseconds (cf., Figure 1c). TEM studies at atomic resolution hardly reach the sub-millisecond range. New developments of time-resolved TEM with a continuous electron beam such as deflector systems that acquire a short sequence of exposures on the camera sensor[158] or the chopping of the electron beam[159] may allow further improvements of the temporal resolution toward the microsecond scale. However, the short exposure times require extremely intense illumination conditions which increase the dose rate and speed up the associated irradiation phenomena. Ultrafast TEM[160] working in a pump-probe approach with laser excitation of the specimen and successive photoelectron pulses is not applicable because the achievable spatial resolution in the single-shot

© 2024 The Authors. Small published by Wiley-VCH GmbH

approach (which is necessary for irreversible transformations) is far from reaching the atomic scale.[161,162]

Therefore, we can conclude that the dynamics of single atoms during the displacement process and subsequent rearrangement of the lattice in the femto- to picosecond regime will remain restricted to atomistic simulations. Short-lived configurations of atoms within the defects and transient states occur in the femto- or picosecond regime. Experimental techniques with sufficient combined spatial and temporal resolution are not in sight today. On the other hand, thermal processes occurring after the atom displacements and including long-range atom migration are orders of magnitude slower and therefore observable in TEM studies. Nevertheless, by improving the temporal resolution of in situ TEM and increasing the computing power in simulations, the gap between the experimentally and theoretically accessible timescales could close in the near future and allow us to gain detailed insight into the mechanisms of defect formation under electron irradiation.

Acknowledgements

The author is very grateful to Pulickel M. Ajayan, to whom this special issue was dedicated, for the long-lasting collaboration. Ajayan's expertise and intuition were of great benefit to the author's research in the field of carbon nanomaterials. The author is also grateful to many colleagues, postdocs, and Ph.D. students, too many to mention all of them here, who have contributed with their work over the decades of research on carbon nanomaterials. During the preparation of this manuscript, valuable discussions with Arkady Krasheninnikov and Jani Kotakoski have been very helpful.

Conflict of Interest

The authors declare no conflict of interest.

Keywords

carbon nanomaterials, electron irradiation, electron microscopy, low-dimensional materials

Received: November 15, 2023
Revised: April 19, 2024
Published online:

[1] H. W. Kroto, J. R. Heath, S. C. O'Brien, R. F. Curl, R. E. Smalley, *Nature* **1985**, *318*, 162.
[2] R. D. Heidenreich, W. M. Hess, L. L. Ban, *J. Appl. Crystallogr.* **1968**, *1*, 1.
[3] W. Krätschmer, L. D. Lamb, K. H. D. R. Fostiropoulos, D. R. Huffman, *Nature* **1990**, *347*, 354.
[4] G. E. Scuseria, *Science* **1996**, *271*, 942.
[5] S. Iijima, *Nature* **1991**, *354*, 56.
[6] P. M. Ajayan, T. W. Ebbesen, *Rep. Prog. Phys.* **1997**, *60*, 1025.
[7] K. S. Novoselov, A. K. Geim, S. V. Morozov, D. E. Jiang, Y. Zhang, S. V. Dubonos, I. V. Grigorieva, A. A. Firsov, *Science* **2004**, *306*, 666.
[8] H. Terrones, M. Terrones, W. K. Hsu, *Chem. Soc. Rev.* **1995**, *24*, 341.
[9] M. Terrones, W. K. Hsu, J. P. Hare, H. W. Kroto, H. Terrones, D. R. M. Walton, *Phil. Trans. R. Soc. A* **1996**, *354*, 2025.
[10] D. Ugarte, *Nature* **1992**, *359*, 707.
[11] P. M. Ajayan, C. Colliex, P. Bernier, J. M. Lambert, *Microsc. Microanal. Microstruct.* **1993**, *4*, 501.
[12] R. F. Egerton, P. Li, M. Malac, *Micron* **2004**, *35*, 399.
[13] R. F. Egerton, *Microsc. Res. Tech.* **2012**, *75*, 1550.
[14] R. F. Egerton, *Microsc. Today* **2021**, *29*, 56.
[15] S. Helveg, C. López-Cartes, J. Sehested, P. L. Hansen, B. S. Clausen, J. R. Rostrup-Nielsen, F. Abild-Petersen, J. K. Nørskov, *Nature* **2004**, *427*, 426.
[16] O. L. Krivanek, M. F. Chisholm, V. Nicolosi, T. J. Pennycook, G. J. Corbin, N. Dellby, M. F. Murfitt, C. S. Own, Z. S. Szilagyi, M. P. Oxley, S. T. Pantelides, S. J. Pennycook, *Nature* **2010**, *464*, 571.
[17] C. Su, M. Tripathi, Q. B. Yan, Z. Wang, Z. Zhang, C. Hofer, H. Wang, L. Basile, G. Su, M. Dong, J. C. Meyer, J. Kotakoski, J. Kong, J. C. Idrobo, T. Susi, J. Li, *Sci. Adv.* **2019**, *5*, eaav2252.
[18] A. V. Krasheninnikov, F. Banhart, *Nat. Mater.* **2007**, *6*, 723.
[19] F. Banhart, J. Kotakoski, A. V. Krasheninnikov, *ACS Nano* **2011**, *5*, 26.
[20] A. V. Krasheninnikov, F. Banhart, J. X. Li, A. S. Forster, R. M. Nieminen, *Phys. Rev. B* **2005**, *72*, 125428.
[21] W. A. McKinley Jr., H. Feshbach, *Phys. Rev.* **1948**, *74*, 1759.
[22] H. Ullmaier, P. Ehrhart, P. Jung, H. Schultz, *Numerical Data and Functional Relationships in Science and Technology–New Series/Condensed Matter*, Springer, Berlin Heidelberg, **1991**.
[23] J. C. Meyer, F. Eder, S. Kurasch, V. Skakalova, J. Kotakoski, H. J. Park, S. Roth, A. Chuvilin, S. Eyhusen, G. Benner, A. Krasheninnikov, U. Kaiser, *Phys. Rev. Lett.* **2012**, *108*, 196102.
[24] F. Banhart, *Rep. Progr. Phys.* **1999**, *62*, 1181.
[25] G. L. Montet, G. E. Myers, *Carbon* **1971**, *9*, 179.
[26] R. F. Egerton, *Philos. Mag.* **1977**, *35*, 1425.
[27] L. Sun, F. Banhart, J. Warner, *MRS Bull.* **2015**, *40*, 29.
[28] F. Vuković, J. M. Leyssale, P. Aurel, N. A. Marks, *Phys. Rev. Appl.* **2018**, *10*, 064040.
[29] C. P. Ewels, R. H. Telling, R. A. A. El-Barbary, M. I. Heggie, P. R. Briddon, *Phys. Rev. Lett.* **2003**, *91*, 025505.
[30] U. Kaiser, J. Biskupek, J. C. Meyer, J. Leschner, L. Lechner, H. Rose, M. Stöger-Pollach, A. N. Khlobystov, P. Hartel, H. Müller, M. Haider, S. Eyhusen, G. Benner, *Ultramicroscopy* **2011**, *111*, 1239.
[31] A. A. El-Barbary, R. H. Telling, C. P. Ewels, M. I. Heggie, P. R. Briddon, *Phys. Rev. B* **2003**, *68*, 144107.
[32] J. Kotakoski, C. Mangler, J. C. Meyer, *Nat. Commun.* **2014**, *5*, 3991.
[33] P. Börner, U. Kaiser, O. Lehtinen, *Phys. Rev. B* **2016**, *93*, 134104.
[34] K. Nordlund, S. J. Zinkle, A. E. Sand, F. Granberg, R. S. Averback, R. Stoller, T. Suzudo, L. Malerba, F. Banhart, W. Weber, F. Willaime, S. L. Dudarev, D. Simeone, *Nat. Commun.* **2018**, *9*, 1084.
[35] T. Susi, D. Kepaptsoglou, Y. C. Lin, Q. M. Ramasse, J. C. Meyer, K. Suenaga, J. Kotakoski, *2D Mater.* **2017**, *4*, 042004.
[36] T. Susi, C. Hofer, G. Argentero, G. T. Leuthner, T. J. Pennycook, C. Mangler, J. C. Meyer, J. Kotakoski, *Nat. Commun.* **2016**, *7*, 13040.
[37] A. Chirita, A. Markevich, M. Tripathi, N. A. Pike, M. J. Verstraete, J. Kotakoski, T. Susi, *Phys. Rev. B* **2022**, *105*, 235419.
[38] A. Zobelli, A. Gloter, C. P. Ewels, G. Seifert, C. Colliex, *Phys. Rev. B* **2007**, *75*, 245402.
[39] P. A. Thrower, in *Chemistry and Physics of Carbon*, (Ed: P.L. Walker, Jr.) Dekker, New York **1969**, Vol. *5*, p. 262
[40] A. J. Stone, D. J. Wales, *J. Chem. Phys. Lett.* **1986**, *128*, 501.
[41] O. V. Yazyev, I. Tavernelli, U. Rothlisberger, L. Helm, *Phys. Rev. B* **2007**, *75*, 115418.
[42] J. Kotakoski, J. C. Meyer, S. Kurasch, D. Santos-Cottin, U. Kaiser, A. V. Krasheninnikov, *Phys. Rev. B* **2011**, *83*, 245420.
[43] C. J. Russo, J. A. Golovchenko, *Proc. Nat. Acad. Sci.* **2012**, *109*, 5953.
[44] J. Kotakoski, D. Santos-Cottin, A. V. Krasheninnikov, *ACS Nano* **2012**, *6*, 671.
[45] O. Dyck, S. Kim, E. Jimenez-Izal, A. N. Alexandrova, S. V. Kalinin, S. Jesse, *Small* **2018**, *14*, 1801771.

 © 2024 The Authors. Small published by Wiley-VCH GmbH

[46] Ç. O. Girit, J. C. Meyer, R. Erni, M. D. Rossell, C. Kisielowski, L. Yang, C.-H. Park, M. F. Crommie, M. L. Cohen, S. G. Louie, A. Zettl, *Science* **2009**, *323*, 1705.
[47] G. T. Leuthner, T. Susi, C. Mangler, J. C. Meyer, J. Kotakoski, *2D Mater.* **2021**, *8*, 035023.
[48] D. Kepaptsoglou, T. P. Hardcastle, C. R. Seabourne, U. Bangert, R. Zan, J. A. Amani, H. Hofsäss, R. J. Nicholls, R. D. M. Brydson, A. J. Scott, Q. M. Ramasse, *ACS Nano* **2015**, *9*, 11398.
[49] T. Susi, J. C. Meyer, J. Kotakoski, *Ultramicroscopy* **2017**, *180*, 163.
[50] Q. Xu, M. Y. Wu, G. F. Schneider, L. Houben, S. K. Malladi, C. Dekker, E. Yucelen, R. E. Dunin-Borkowski, H. W. Zandbergen, *ACS Nano* **2013**, *7*, 1566.
[51] K. M. Roccapriore, M. G. Boebinger, O. Dyck, A. Ghosh, R. R. Unocic, S. V. Kalinin, M. Ziatdinov, *ACS Nano* **2022**, *16*, 17116.
[52] M. I. Heggie, *J. Phys.: Condens. Matter* **1991**, *3*, 3065.
[53] R. H. Telling, C. P. Ewels, A. A. El-Barbary, M. I. Heggie, *Nat. Mater.* **2003**, *2*, 333.
[54] R. Zan, Q. M. Ramasse, R. Jalil, T. Georgiou, U. Bangert, K. S. Novoselov, *ACS Nano* **2013**, *7*, 10167.
[55] G. Algara-Siller, S. Kurasch, M. Sedighi, O. Lehtinen, U. Kaiser, *Appl. Phys. Lett.* **2013**, *103*, 203107.
[56] S. T. Skowron, S. L. Roberts, A. N. Khlobystov, E. Besley, *Micron* **2019**, *120*, 96.
[57] L. Vicarelli, S. J. Heerema, C. Dekker, H. W. Zandbergen, *ACS Nano* **2015**, *9*, 3428.
[58] P. A. Thrower, R. M. Mayer, *Phys. Status Solidi A* **1978**, *47*, 11.
[59] S. Johns, T. Poulsen, J. J. Kane, W. E. Windes, R. Ubic, C. Karthik, *Carbon* **2019**, *143*, 908.
[60] J. Ma, D. Alfè, A. Michaelides, E. Wang, *Phys. Rev. B* **2009**, *80*, 033407.
[61] L. Li, S. Reich, J. Robertson, *Phys. Rev. B* **2005**, *72*, 184109.
[62] J. Kotakoski, A. V. Krasheninnikov, U. Kaiser, J. C. Meyer, *Phys. Rev. Lett.* **2011**, *106*, 105505.
[63] A. W. Robertson, B. Montanari, K. He, C. S. Allen, Y. A. Wu, N. M. Harrison, A. Kirkland, J. H. Warner, *ACS Nano* **2013**, *7*, 4495.
[64] J. Kotakoski, A. Krasheninnikov, in *Computational Nanoscience*, (Ed: E. Bichoutskaia) RSC Publishing, Burlington House, Piccadilly, London **2011**.
[65] A. V. Krasheninnikov, P. O. Lehtinen, A. S. Foster, R. M. Nieminen, *Chem. Phys. Lett.* **2006**, *418*, 132.
[66] A. V. Krasheninnikov, *J. Comput. Theor. Nanosci.* **2008**, *5*, 1828.
[67] A. Postl, P. P. P. Hilgert, A. Markevich, J. Madsen, K. Mustonen, J. Kotakoski, T. Susi, *Carbon* **2022**, *196*, 596.
[68] F. Banhart, P. M. Ajayan, *Nature* **1996**, *382*, 433.
[69] F. Banhart, T. Füller, P. Redlich, P. M. Ajayan, *Chem. Phys. Lett.* **1997**, *269*, 349.
[70] A. Hashimoto, K. Suenaga, A. Gloter, K. Urita, S. Iijima, *Nature* **2004**, *430*, 870.
[71] M. H. Gass, U. Bangert, A. L. Bleloch, P. Wang, R. R. Nair, A. K. Geim, *Nat. Nanotechnol.* **2008**, *3*, 676.
[72] J. C. Meyer, C. Kisielowski, R. Erni, M. D. Rossell, M. F. Crommie, A. Zettl, *Nano Lett.* **2008**, *8*, 3582.
[73] Y. Kim, J. Ihm, E. Yoon, G. D. Lee, *Phys. Rev. B* **2011**, *84*, 075445.
[74] J. H. Warner, G. D. Lee, K. He, A. W. Robertson, E. Yoon, A. I. Kirkland, *ACS Nano* **2013**, *7*, 9860.
[75] A. W. Robertson, G. D. Lee, K. He, E. Yoon, A. I. Kirkland, J. H. Warner, *Nano Lett.* **2014**, *14*, 1634.
[76] O. Lehtinen, N. Vats, G. Algara-Siller, P. Knyrim, U. Kaiser, *Nano Lett.* **2015**, *15*, 235.
[77] C. T. Toh, H. Zhang, J. Lin, A. S. Mayorov, Y. P. Wang, C. M. Orofeo, D. B. Ferry, H. Andersen, N. Kakenov, Z. Guo, I. H. Abidi, H. Sims, K. Suenaga, S. Pantelides, B. Özyilmaz, *Nature* **2020**, *577*, 199.
[78] C. P. Ewels, M. I. Heggie, P. R. Briddon, *Chem. Phys. Lett.* **2002**, *351*, 178.
[79] A. Gulans, A. V. Krasheninnikov, M. J. Puska, R. M. Nieminen, *Phys. Rev. B* **2011**, *84*, 024114.
[80] L. Tsetseris, S. T. Pantelides, *Carbon* **2009**, *47*, 901.
[81] Y. H. Lee, S. G. Kim, D. Tománek, *Phys. Rev. Lett.* **1997**, *78*, 2393.
[82] P. O. Lehtinen, A. S. Foster, A. Ayuela, A. Krasheninnikov, K. Nordlund, R. M. Nieminen, *Phys. Rev. Lett.* **2003**, *91*, 017202.
[83] Y. Ma, *Phys. Rev. B* **2007**, *76*, 075419.
[84] M. T. Lusk, L. D. Carr, *Phys. Rev. Lett.* **2008**, *100*, 175503.
[85] M. D. Lusk, D. T. Wu, L. D. Carr, *Phys. Rev. B* **2010**, *81*, 155444.
[86] K. Cao, S. T. Skowron, C. T. Stoppiello, J. Biskupek, A. N. Khlobystov, U. Kaiser, *Angew. Chem., Int. Ed.* **2020**, *59*, 22922.
[87] F. Banhart, *J. Appl. Phys.* **1997**, *81*, 3440.
[88] B. Song, G. F. Schneider, Q. Xu, G. Pandraud, C. Dekker, H. Zandbergen, *Nano Lett.* **2011**, *11*, 2247.
[89] R. Zan, Q. M. Ramasse, U. Bangert, K. S. Novoselov, *Nano Lett.* **2012**, *12*, 3936.
[90] B. Zhang, L. Zhao, Y. Cheng, D. Golberg, M. S. Wang, *Nano Lett.* **2016**, *16*, 5221.
[91] X. Li, Y. Cheng, L. Zhao, Q. Zhang, M. S. Wang, *Carbon* **2018**, *133*, 186.
[92] Y. Cheng, X. Li, H. Gao, J. Wang, G. Luo, D. Golberg, M. S. Wang, *Carbon* **2020**, *160*, 98.
[93] P. M. Ajayan, S. Iijima, *Nature* **1993**, *361*, 333.
[94] V. H. Crespi, N. G. Chopra, M. L. Cohen, A. Zettl, S. G. Louie, *Phys. Rev. B* **1996**, *54*, 5927.
[95] P. M. Ajayan, V. Ravikumar, J.-C. Charlier, *Phys. Rev. Lett.* **1998**, *81*, 1437.
[96] Z. Lin, G. Shao, W. Liu, Y. Wang, H. Wang, H. Wang, B. Fan, H. Lu, H. Xu, R. Zhang, *Carbon* **2022**, *192*, 356.
[97] J. Koike, D. F. Pedraza, *J. Mater. Res.* **1994**, *9*, 1899.
[98] M. Duchamp, R. Meunier, R. Smajda, M. Mionic, A. Magrez, J. W. Seo, L. Forró, B. Song, D. Tománek, *J. Appl. Phys.* **2010**, *108*, 084314.
[99] J. A. Rodriguez-Manzo, F. Banhart, *Nano Lett.* **2009**, *9*, 2285.
[100] S. Trasobares, O. Stephan, C. Colliex, G. Hug, W. K. Hsu, H. W. Kroto, D. R. M. Walton, *Eur. Phys. J. B* **2001**, *22*, 117.
[101] B. W. Smith, D. E. Luzzi, *J. Appl. Phys.* **2001**, *90*, 3509.
[102] J. H. Warner, F. Schäffel, G. Zhong, M. H. Rümmeli, B. Büchner, J. Robertson, G. A. D. Briggs, *ACS Nano* **2009**, *3*, 1557.
[103] E. Hernandez, V. Meunier, B. W. Smith, R. Rurali, H. Terrones, M. Buongiorno Nardelli, D. E. Luzzi, J.-C. Charlier, *Nano Lett.* **2003**, *3*, 1037.
[104] J. H. Warner, Y. Ito, M. Zaka, L. Ge, T. Akachi, H. Okimoto, K. Porfyrakis, A. A. R. Watt, H. Shinohara, G. A. D. Briggs, *Nano Lett.* **2008**, *8*, 2328.
[105] J. X. Li, F. Banhart, *Nano Lett.* **2004**, *4*, 1143.
[106] Y. Gan, J. Kotakoski, A. V. Krasheninnikov, K. Nordlund, F. Banhart, *New J. Phys.* **2008**, *10*, 023022.
[107] F. Banhart, J. X. Li, A. V. Krasheninnikov, *Phys. Rev. B* **2005**, *71*, 241408.
[108] M. Terrones, H. Terrones, F. Banhart, J.-C. Charlier, P. M. Ajayan, *Science* **2000**, *288*, 1226.
[109] M. Terrones, F. Banhart, N. Grobert, J.-C. Charlier, H. Terrones, P. M. Ajayan, *Phys. Rev. Lett.* **2002**, *89*, 075505.
[110] T. D. Yuzvinsky, W. Mickelson, S. Aloni, G. E. Begtrup, A. Kis, A. Zettl, *Nano Lett.* **2006**, *6*, 2718.
[111] L. Sun, F. Banhart, A. V. Krasheninnikov, J. A. Rodriguez-Manzo, M. Terrones, P. M. Ajayan, *Science* **2006**, *312*, 1199.
[112] L. Sun, A. V. Krasheninnikov, T. Ahlgren, K. Nordlund, F. Banhart, *Phys. Rev. Lett.* **2008**, *101*, 156101.
[113] T. Aref, M. Remeika, A. Bezryadin, *J. Appl. Phys.* **2008**, *104*, 024312.
[114] S. Iijima, *J. Cryst. Growth* **1980**, *50*, 675.
[115] H. Terrones, M. Terrones, *J. Phys. Chem. Solids* **1997**, *58*, 1789.
[116] H. Terrones, M. Terrones, *Phys. Rev. B* **1997**, *55*, 9969.
[117] Y. Saito, T. Yoshikawa, M. Inagaki, M. Tomita, T. Hayashi, *Chem. Phys. Lett.* **1993**, *204*, 277.
[118] K. R. Bates, G. E. Scuseria, *Theor. Chem. Acc.* **1998**, *99*, 29.
[119] D. Ugarte, *Chem. Phys. Lett.* **1993**, *207*, 473.

 © 2024 The Authors. Small published by Wiley-VCH GmbH

[120] M. Zaiser, S. Chartier, *arXiv* **2010**, *1009*, 4035.
[121] E. Akatyeva, J. Y. Huang, T. Dumitrică, *Phys. Rev. Lett.* **2010**, *105*, 106102.
[122] D. Ugarte, *Chem. Phys. Lett.* **1993**, *209*, 99.
[123] Y. Saito, T. Matsumoto, K. Nishikubo, *J. Cryst. Growth* **1997**, *172*, 163.
[124] F. Banhart, P. Redlich, P. M. Ajayan, *Chem. Phys. Lett.* **1998**, *292*, 554.
[125] F. Banhart, J.-C. Charlier, P. M. Ajayan, *Phys. Rev. Lett.* **2000**, *84*, 686.
[126] J. Y. Huang, *Nano Lett.* **2007**, *7*, 2335.
[127] Y. Lyutovich, F. Banhart, *Appl. Phys. Lett.* **1999**, *74*, 659.
[128] V. L. Kuznetsov, A. L. Chuvilin, Y. V. Butenko, I. Y. Mal'kov, V. M. Titov, *Chem. Phys. Lett.* **1994**, *222*, 343.
[129] V. V. Roddatis, V. L. Kuznetsov, Y. V. Butenko, D. S. Su, R. Schlögl, *Phys. Chem. Chem. Phys.* **2002**, *4*, 1964.
[130] M. Zaiser, F. Banhart, *Phys. Rev. Lett.* **1997**, *79*, 3680.
[131] M. Zaiser, Y. Lyutovich, F. Banhart, *Phys. Rev. B* **2000**, *62*, 3058.
[132] C. S. Casari, M. Tommasini, R. R. Tykwinski, A. Milani, *Nanoscale* **2016**, *8*, 4414.
[133] F. Banhart, *Beilstein J. Nanotechnol.* **2015**, *6*, 559.
[134] H. E. Troiani, M. Miki-Yoshida, G. A. Camacho-Bragado, M. A. L. Marques, A. Rubio, J. A. Ascencio, M. Jose-Yacaman, *Nano Lett.* **2003**, *3*, 751.
[135] C. Jin, H. Lan, L. Peng, K. Suenaga, S. Iijima, *Phys. Rev. Lett.* **2009**, *102*, 205501.
[136] A. Chuvilin, J. C. Meyer, G. Algara-Siller, U. Kaiser, *New J. Phys.* **2009**, *11*, 083019.
[137] O. Cretu, A. R. Botello-Mendez, I. Janowska, C. Pham-Huu, J.-C. Charlier, F. Banhart, *Nano Lett.* **2013**, *13*, 3487.
[138] Y. C. Lin, S. Morishita, M. Koshino, C. H. Yeh, P. Y. Teng, P. W. Chiu, H. Sawada, K. Suenaga, *Nano Lett.* **2017**, *17*, 494.
[139] M. Liu, V. I. Artyukhov, H. Lee, F. Xu, B. I. Yakobson, *ACS Nano* **2013**, *7*, 10075.
[140] A. La Torre, A. Botello-Mendez, W. Baaziz, J.-C. Charlier, F. Banhart, *Nat. Commun.* **2015**, *6*, 6636.
[141] M. Kumar, Y. Ando, *J. Nanosci. Nanotechnol.* **2010**, *10*, 3739.
[142] H. Ago, Y. Ogawa, M. Tsuji, S. Mizuno, H. Hibino, *J. Phys. Chem. Lett.* **2012**, *3*, 2228.
[143] A. Yasuda, N. Kawase, W. Mizutani, *J. Phys. Chem. B* **2002**, *106*, 13294.
[144] J. A. Rodríguez-Manzo, A. Tolvanen, A. V. Krasheninnikov, K. Nordlund, A. Demortière, F. Banhart, *Nanoscale* **2010**, *2*, 901.
[145] J. A. Rodríguez-Manzo, F. Banhart, M. Terrones, H. Terrones, N. Grobert, P. M. Ajayan, B. G. Sumpter, V. Meunier, M. Wang, Y. Bando, D. Golberg, *Proc. Nat. Acad. Sci.* **2009**, *106*, 4591.
[146] J. A. Rodríguez-Manzo, M. S. Wang, F. Banhart, Y. Bando, D. Golberg, *Adv. Mater.* **2009**, *21*, 4477.
[147] Q. M. Ramasse, R. Zan, U. Bangert, D. W. Boukhvalov, Y. W. Son, K. Novoselov, *ACS Nano* **2012**, *6*, 4063.
[148] V. I. Lebedeva, T. W. Chamberlain, A. M. Popov, A. A. Knizhnik, T. Zoberbier, J. Biskupek, U. Kaiser, A. Khlobystov, *Nanoscale* **2014**, *6*, 14877.
[149] A. Leonhardt, M. Ritschel, R. Kozhuharova, A. Graff, T. Mühl, R. Huhle, L. Mönch, D. Elefant, C. M. Schneider, *Diamond Relat. Mater.* **2003**, *12*, 790.
[150] J. A. Rodríguez-Manzo, M. Terrones, H. Terrones, H. W. Kroto, L. Sun, F. Banhart, *Nat. Nanotechnol.* **2007**, *2*, 307.
[151] J. A. Rodríguez-Manzo, I. Janowska, C. Pham-Huu, A. Tolvanen, A. V. Krasheninnikov, K. Nordlund, F. Banhart, *Small* **2009**, *5*, 2710.
[152] R. Arenal, A. Lopez-Bezanilla, *ACS Nano* **2014**, *8*, 8419.
[153] J. A. Rodríguez-Manzo, C. Pham-Huu, F. Banhart, *ACS Nano* **2011**, *5*, 1529.
[154] J. A. Rodríguez-Manzo, F. Banhart, *Appl. Phys. Lett.* **2011**, *98*, 183105.
[155] O. Cretu, J. A. Rodríguez-Manzo, A. Demortiere, F. Banhart, *Carbon* **2012**, *50*, 259.
[156] F. Börrnert, S. M. Avdoshenko, A. Bachmatiuk, I. Ibrahim, B. Büchner, G. Cuniberti, M. H. Rümmeli, *Adv. Mater.* **2012**, *24*, 5630.
[157] L. Zhao, H. Q. Ta, A. Dianat, A. Soni, A. Fediai, W. Yin, T. Gemming, B. Trzebicka, G. Cuniberti, Z. Liu, A. Bachmatiuk, M. H. Rümmeli, *Nano Lett.* **2017**, *17*, 4725.
[158] T. LaGrange, B. W. Reed, M. K. Santala, J. T. McKeown, A. Kulovits, J. M. K. Wiezorek, L. Nikolova, F. Rosei, B. J. Siwick, G. H. Campbell, *Micron* **2012**, *43*, 1108.
[159] L. Zhang, J. P. Hoogenboom, B. Cook, B. Kruit, *Struct. Dyn.* **2019**, *6*, 051501.
[160] A. Zewail, *Science* **2010**, *328*, 187.
[161] W. E. King, G. H. Campbell, A. Frank, B. Reed, J. F. Schmerge, B. J. Siwick, B. C. Stuart, P. M. Weber, *J. Appl. Phys.* **2005**, *97*, 111101.
[162] M. Picher, K. Bücker, T. LaGrange, F. Banhart, *Ultramicroscopy* **2018**, *188*, 41.

Florian Banhart obtained his Ph.D. from the University of Stuttgart (Germany) in 1988. He was a research scientist at the Max Planck Institute for Metal Research in Stuttgart and at the University of Ulm. He was appointed as a professor of physical chemistry at the University of Mainz (Germany) in 2003 and as a professor of physics at the University of Strasbourg (France) in 2007. He is an honorary member of the Institut Universitaire de France. His research activities are in the microscopic characterization of nanomaterials.

© 2024 The Authors. Small published by Wiley-VCH GmbH